PERGAMON

Journal of Structural Geology 23 (2001) 1971–1995

JOURNAL OF STRUCTURAL GEOLOGY

www.elsevier.com/locate/jstrugeo

Structural evolution within the Luning–Fencemaker fold-thrust belt, Nevada: progression from back-arc basin closure to intra-arc shortening

Sandra J. Wyld*, Johannah W. Rogers[1], James E. Wright

Department of Geology, University of Georgia, Athens, GA 30602, USA

Received 12 November 1999; revised 24 October 2000; accepted 21 February 2001

Abstract

The Luning–Fencemaker fold-thrust belt (LFTB) of central Nevada reflects major Mesozoic shortening in the western US Cordillera, and involved contractional deformation in Triassic and lower Jurassic back-arc basinal strata. Structural analyses in the Santa Rosa Range, in the northern LFTB, provide new insight into the evolution of this belt. Four phases of deformation are recognized in the Santa Rosa Range. D_1 involved tight to isoclinal folding, cleavage development under low-grade metamorphic conditions, and reverse faulting. This deformation phase reflects NW–SE shortening of $\geqq 55$–70% in the Early and/or Middle Jurassic. D_2 structures are similar in orientation to D_1 but involved much less overall strain and are well developed only to the southeast. D_2 appears to be related to thrusting along the eastern margin of the LFTB in the Middle and/or Late Jurassic. D_3 deformation reflects very minor shortening ($<5\%$) in a subvertical direction, and is tentatively interpreted to reflect stresses generated during initial intrusion of mid-Cretaceous plutons in the area. D_4 deformation demonstrably occurred synchronously with emplacement of Cretaceous granitoids dated at 102 Ma (U–Pb zircon) based on syntectonic relations between D_4 structures and thermal metamorphism associated with intrusion, and an upgrade in D_4 strain in the thermally softened metamorphic aureoles of the intrusions. This last phase of deformation reflects minor regional NE–SW shortening, coupled with localized strain associated with pluton emplacement.

Formation of the LFTB structural province was accomplished during the D_1 and D_2 phases of deformation, and most shortening occurred during the D_1 event. This Jurassic deformation led to structural closure of the back-arc basin by top-to-the-SE tectonic transport and development of a largely ductile fold-thrust belt. Subsequent deformation (D_3 and D_4) is >50 m.y. younger and unrelated to development of the LFTB. The younger deformation reflects a combination of minor regional shortening, interpreted to be related to the Cretaceous Sevier orogeny, plus localized shortening related to emplacement of Cretaceous intrusions.

Keywords: Luning–Fencemaker fold-thrust belt; Back-arc basin closure; Intra-arc shortening

1. Introduction

The Luning–Fencemaker fold-and-thrust belt (LFTB) of north-central Nevada (Fig. 1) accommodated significant Mesozoic shortening in the Cordillera of the western United States (Oldow, 1984; Burchfiel et al., 1992). Deformation occurred primarily in early Mesozoic sedimentary strata that were deposited in a deep marine back-arc basin between a volcanic arc to the west and the continental shelf to the east (Fig. 1; Speed, 1978; Wyld, 2000).

Oldow (1984) was the first to propose a regional framework for the structural evolution of the LFTB. Based on detailed studies in the southern LFTB and more reconnaissance studies in the northern LFTB, he concluded that three to four phases of deformation could be recognized within the belt, each of which involved folding ± reverse faulting and cleavage development. Oldow (1984) emphasized that the timing of different phases of deformation was poorly constrained, but concluded, based on available geochronologic constraints, that the first phase began in the Early to Middle Jurassic, the second phase began in the Middle to Late Jurassic and continued into the Early Cretaceous (post-102 Ma), and that all deformation was completed by the mid-Cretaceous (~100–90 Ma). The LFTB was therefore envisioned as developing progressively over a period of some 100 m.y., apparently in a manner similar to that seen in other long-lived fold-thrust belts.

Since this analysis, few other detailed studies have been done in the LFTB, and this has hindered our ability to characterize the structural evolution of the belt. In this

* Corresponding author. Tel.: +1-706-542-9908; fax: +1-706-542-2425.
E-mail address: swyld@gly.uga.edu (S.J. Wyld).
[1] Now at CH_2M Hill, 115 Perimeter Center Place, NE, Suite 700, Atlanta, GA 30346, USA.

0191-8141/01/$ - see front matter
PII: S0191-8141(01)00042-6

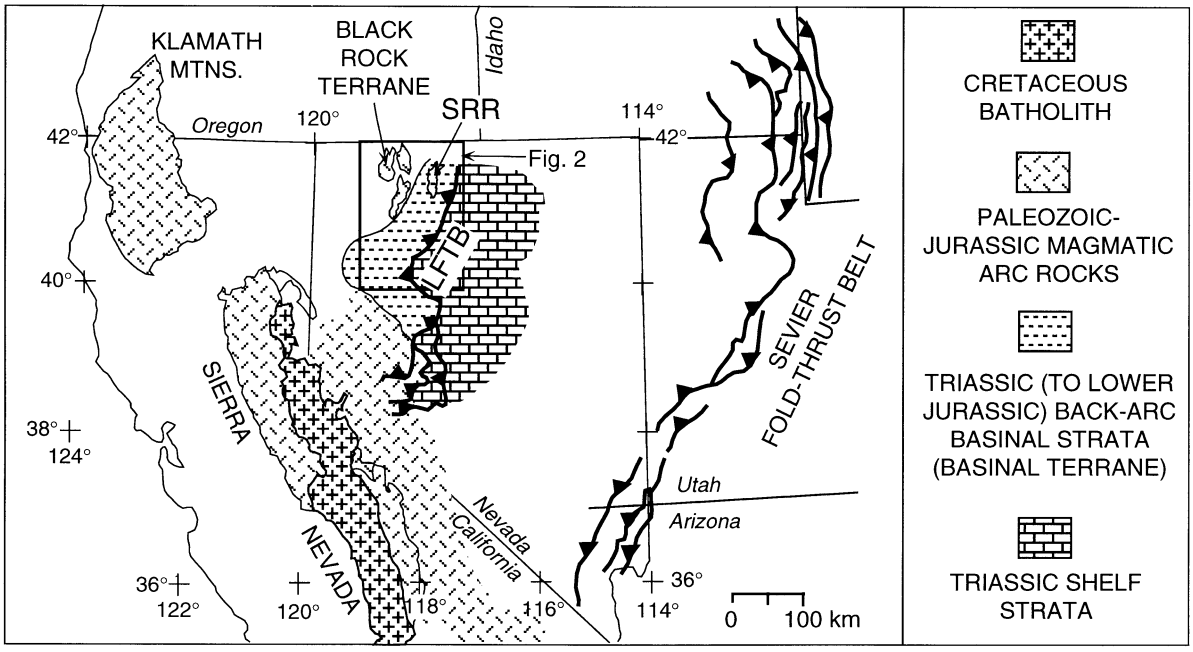

Fig. 1. Early Mesozoic rocks of the western US Cordillera, Cretaceous batholith belt, and location of major Mesozoic fold-and-thrust belts. The Jurassic to Cretaceous(?) Luning–Fencemaker thrust belt (LFTB) encompasses the entire basinal terrane; only frontal thrusts are shown (Oldow, 1984). Sevier fold-and-thrust belt is Cretaceous to Early Tertiary. SRR is the Santa Rosa Range.

study, we define a detailed structural history of basinal rocks in the northern LFTB, with the goal of integrating these data with published studies from elsewhere in the LFTB into a more comprehensive model for the Mesozoic structural evolution of this part of the Cordillera. The focus of our study is the Santa Rosa Range (Figs. 1 and 2). We show that four phases of deformation affected this area, the first two of which reflect structural closure of the back-arc basin during development of the LFTB in the Jurassic, and the last two of which occurred much later in the Cretaceous during intrusion of arc granitoids and the Sevier orogeny.

The northern LFTB is bounded to the east by the Fencemaker thrust (Fig. 2) along which deep marine basinal strata were thrust over coeval shallow marine shelf deposits (Speed, 1978; Oldow, 1984; Elison and Speed, 1989; Oldow et al., 1990). The location of this frontal thrust fault appears to coincide with the position of the early Mesozoic continental slope, and much less Mesozoic shortening is recognized within the shelf strata than in the coeval basinal rocks, indicating that the continental margin acted as a relatively rigid buttress during deformation of the basinal succession (Heck and Speed, 1987; Elison and Speed, 1989; Oldow et al., 1990). To the west, the northern LFTB is bounded by Paleozoic and Mesozoic magmatic arc rocks of the Black Rock terrane (Fig. 2). This volcanic terrane was apparently thrust eastward over the basinal rocks during initial development of the LFTB (Quinn, 1996; Rogers, 1999; Folsom, 2000; Wyld, 2000).

Back-arc basinal strata deformed in the northern LFTB are largely of Upper Triassic (Norian) age, and consist mostly of metamorphosed shale (Compton, 1960; Burke and Silberling, 1973; Speed, 1978; Lupe and Silberling, 1985; Wyld, 2000). The term 'basinal terrane' has been applied to these rocks by Speed (1978), and provides a convenient name that we use throughout the paper. The basin in which these strata were deposited apparently developed in response to an episode of regional extension from the Early to Late Triassic (Wyld, 2000). Locally (east of Lovelock; L in Fig. 2), the Triassic rocks are overlain by shallower marine Lower Jurassic strata (as young as Toarcian) that reflect shoaling of the basin and potentially record the onset of LFTB deformation (Speed, 1974, 1978). As the fold-thrust belt evolved, shortening resulted in structural closure of the Triassic back-arc basin and cessation of deep marine deposition in this part of Nevada (Speed, 1978; Oldow, 1984; Saleeby and Busby-Spera, 1992; Smith et al., 1993), but the northern LFTB continued to occupy a back-arc position through the Late Jurassic, as indicated by the fact that Jurassic plutonic and volcanic rocks are mostly located farther west (Figs. 1 and 2). By the mid-Cretaceous, however, the realm of arc magmatism had spread further east, as a result of which basinal rocks of the northern LFTB are intruded by mid-Cretaceous arc-related granitoid plutons (Fig. 2; Barton et al., 1988).

2. Geologic framework of the Santa Rosa Range

The Santa Rosa Range (SRR) is located in the northernmost part of the LFTB (Fig. 2). Geologic units in the SRR were originally described by Compton (1960) who defined three main rock assemblages: variably metamorphosed and

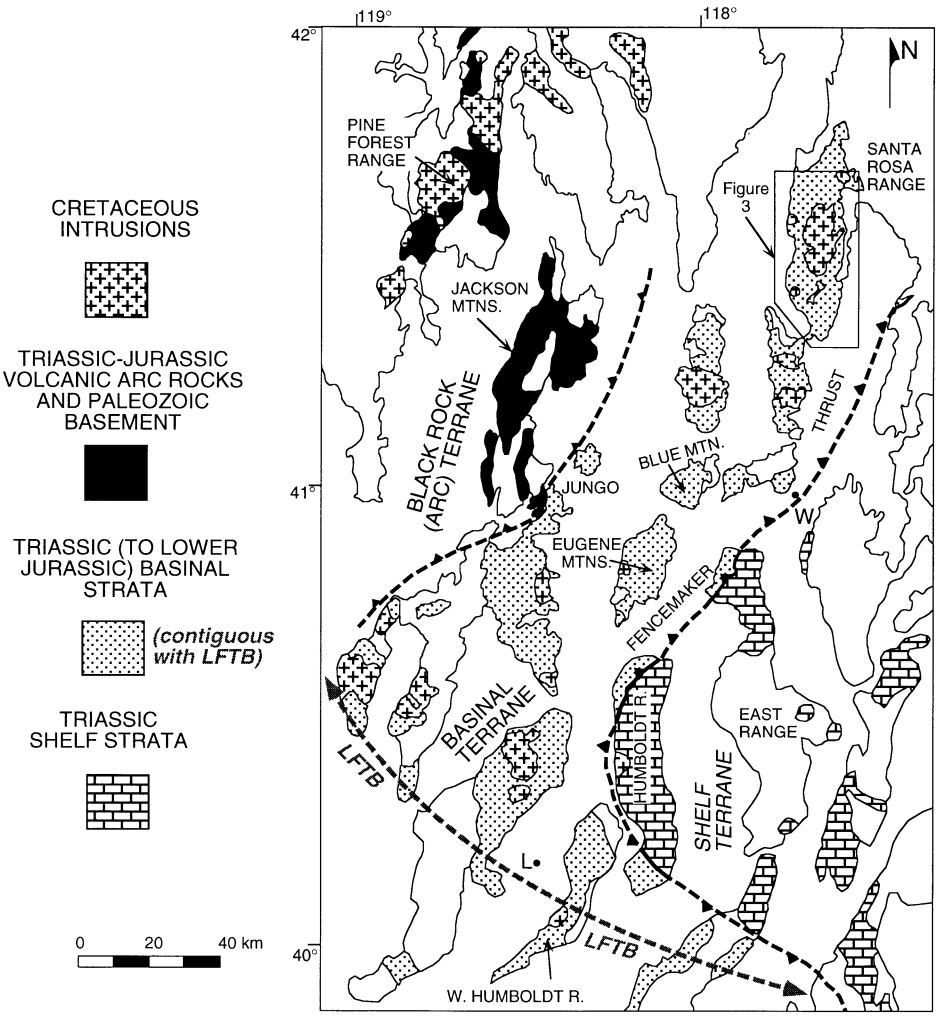

Fig. 2. Location map showing mountain ranges in north-central Nevada (outlined area in Fig. 1), distribution of early Mesozoic rocks of arc, basinal, and shelf terranes, and location of Cretaceous plutons. Non-patterned areas within ranges are Cenozoic in Black Rock and basinal terranes; Cenozoic and Paleozoic in shelf terrane. Non-patterned areas between ranges are Cenozoic valley fill. Modified from Stewart and Carlson (1978), Oldow (1984), Elison and Speed (1989), Wyld (1996, 2000), Quinn et al. (1997) and Folsom (2000). L is Lovelock, and W is Winnemucca.

deformed Triassic sedimentary strata consisting mostly of metamorphosed shale and siltstone; granitoid stocks and dikes of inferred Cretaceous age; and unmetamorphosed and undeformed Tertiary volcanic and sedimentary rocks (Fig. 3). The principal focus of Compton's (1960) study was to map and describe Mesozoic units, and to examine in detail the character and distribution of contact metamorphism associated with the granitoid intrusions; limited emphasis was placed on structural analysis. Subsequent work by Rogers (1999) in the southern SRR (Figs. 3 and 4) focused primarily on a detailed structural and metamorphic analysis of the Triassic rocks, but this study also examined the facies, lithology and composition of the Triassic strata, and the composition, structure and contact relations of the granitoid intrusions, as well as checking for accuracy in the location of Compton's unit contacts.

The Triassic strata in the SRR constitute part of the back-arc basinal succession described in the previous section (Speed, 1978; Lupe and Silberling, 1985; Wyld, 2000). Compton (1960) divided these rocks into six different units, named (from base to top) the Grass Valley, Winnemucca, O'Neill, Singas, Andorno, and Mullinix Formations (Fig. 3), which together have a combined structural thickness of over 6 km. Middle and early late Norian fossils were found in the Winnemucca and Andorno Formations, respectively, and the entire succession is thought to be of Norian age based on comparisons with biostratigraphically dated and lithologically similar rocks elsewhere in the basinal terrane (Compton, 1960; Speed, 1978; Lupe and Silberling, 1985).

The following description of the Triassic units is based on the work of Compton (1960) and Rogers (1999), and emphasizes protolith lithology. Each of the six units is dominated by shale (now slate and phyllite) with less common interlayered siltstone (now silty slate and phyllite), and these two rock types together constitute over 80% of the

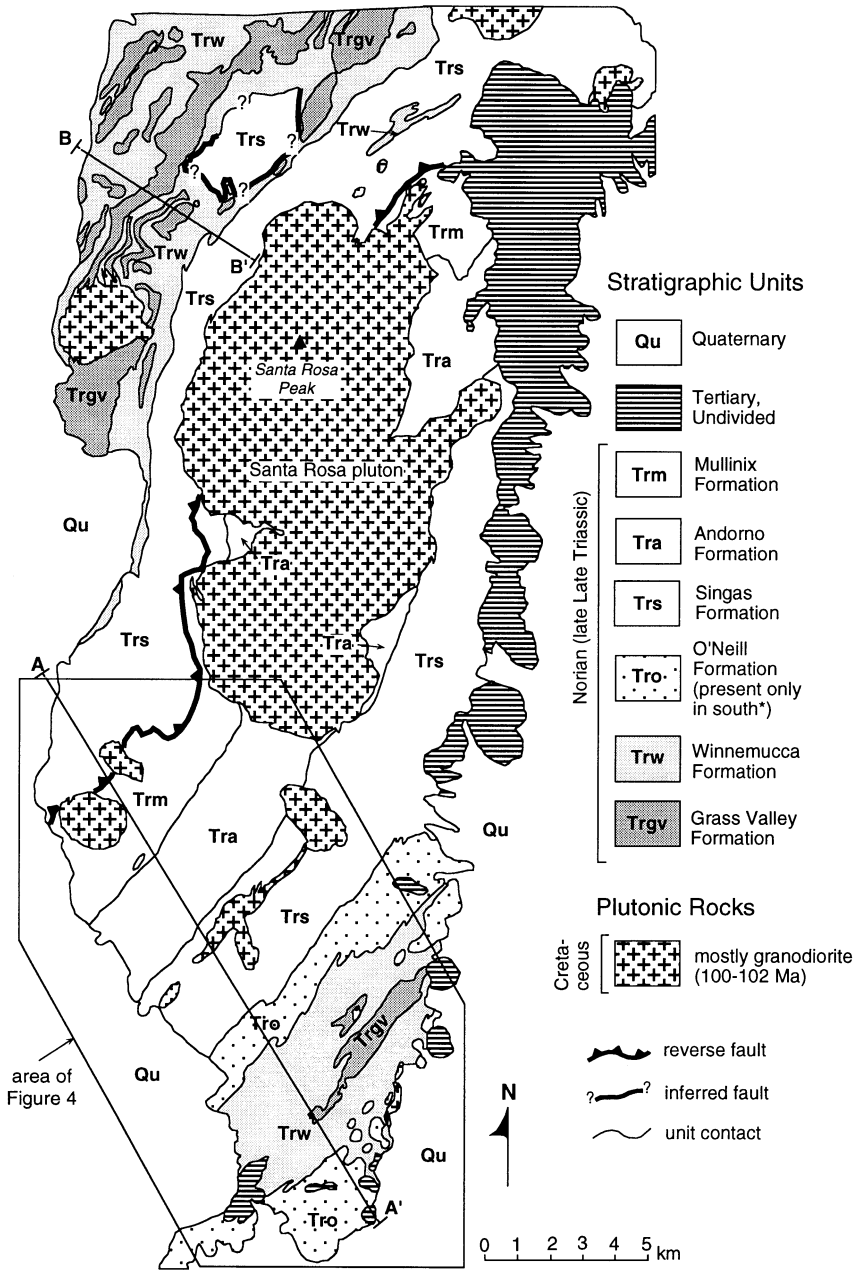

Fig. 3. Geologic map of Santa Rosa Range, modified from Compton (1960). Age data for plutonic rocks cited in text. *According to Compton (1960), the O'Neill Formation either pinches out stratigraphically to the northwest or becomes indistinguishable from the lower Singas Formation.

Triassic succession. Most units (all except the Winnemucca Formation) have variable amounts (up to ~20%) of interlayered, fine- to medium-grained quartz arenite (now quartzite), occurring in beds ranging from 5 cm to 10 m thick. Calcareous rocks are also locally present: the Winnemucca Formation contains abundant calcareous shales and siltstones, and Compton (1960) reports that the Singas and Andorno Formations contain rare limestone interlayers, although none were observed in the southern SRR (Rogers, 1999). Distinction between the different units is based on the abundance of siltstone and sandstone, bedding thickness and sedimentary structures in siltstones and sandstones, and the presence or absence of calcareous rocks (Compton, 1960), and is quite clear despite the fact that all units contain an abundance of similar rock types. Rogers (1999) analyzed the character and distribution of facies within the Triassic strata in the southern SRR and concluded that they were deposited primarily as distal turbidites and hemipelagic deposits in an outer submarine fan to basin plain environment.

Following deposition, the Triassic strata were regionally deformed during development of the LFTB, and then cross-cut by numerous Cretaceous granitoid intrusions (Fig. 3; Compton, 1960; Rogers, 1999). These intrusions are mostly

biotite granodiorite and tonalite, and the largest is the Santa Rosa pluton in the center of the range (Fig. 3). Smaller stocks flank this pluton (Fig. 3), and dikes are scattered throughout the range but are most common near larger intrusions. Based on similarities in mineralogy and geochemistry, Compton (1960) and Rogers (1999) concluded that all these various intrusions are related manifestations of a single intrusive episode. The Santa Rosa pluton was dated by Smith et al. (1971) at ~100 Ma (K/Ar analysis on hornblende and biotite), and we have dated the Andorno stock in the southern SRR (Fig. 4) at 102.4 ± 1.0 Ma (see Section 6). These data support the concept that intrusions in the SRR are all of similar age.

Two phases of metamorphism are recognized in the SRR (Compton, 1960; Rogers, 1999), one of which affects all the Triassic units and occurred during regional deformation prior to mid-Cretaceous plutonism, and the other of which was associated with mid-Cretaceous intrusions and is evident primarily only in the metamorphic aureoles around the intrusions. Rogers (1999) established the metamorphic grade of the earlier regional metamorphism based on petrographic, illite crystallinity, and microprobe analyses of the Triassic slates and phyllites. This study demonstrated that the grade achieved during regional metamorphism was subgreenschist to lower greenschist grade.

Later contact metamorphism locally overprinted the regional metamorphism and produced contact metamorphic aureoles that extend to distances of as much as 2 km around the larger intrusive bodies (Compton, 1960; Rogers, 1999). The most comprehensive data on contact metamorphism in the SRR is that of Compton (1960), whose conclusions were confirmed by the study of Rogers (1999) in the southern SRR. Compton (1960) defined the outer contact of each metamorphic aureole by the first appearance of biotite, andalusite, cordierite, and/or staurolite within metapelitic rocks, and demonstrated that metamorphic facies in the contact aureoles reflect a progression from greenschist grade around the smaller intrusions and in the outer parts of the aureoles around larger intrusions, to upper amphibolite facies near the margins of the larger intrusions. According to Compton (1960), metamorphic assemblages in the aureoles reflect intrusion and metamorphism under pressures of 100–250 MPa, at a depth of 3–8 km, with aureole temperatures ranging from 450 to 600°C, depending on proximity to intrusion margins.

The data presented in this paper focuses on structural relations in the southern SRR (outlined area in Fig. 3). Our goal is to define and analyze all pre-Cenozoic phases of deformation and metamorphism that have affected Triassic strata in the southern SRR. As discussed below, four different phases of Mesozoic deformation are recognized (D_1, D_2, D_3, and D_4), the first and last of which were associated with metamorphism (M_1, M_4). Each phase of deformation is described in the following sections in terms of structures, syntectonic metamorphism, kinematics, degree of shortening, and age constraints. These data are followed by a comparison between Mesozoic structures in the SRR and those in other parts of the northern LFTB, and a revised analysis of the structural evolution of the northern LFTB based on relations in the SRR.

3. D_1 deformation and regional metamorphism

Our work indicates that the principal phase of shortening in the southern SRR is the first, D_1, and that this phase produced the dominant structural fabric seen in the Triassic rocks (Fig. 4). Structures related to D_1 deformation include a pervasive cleavage developed during M_1 regional metamorphism, folds at various scales, and a reverse fault that duplicates the Triassic stratigraphy (Fig. 3). Although these structures predate three other phases of deformation in the southern SRR, the younger deformation generally involved much less strain than D_1, as a result of which the original orientation of D_1 structures is still readily discernible.

3.1. S_1 cleavage and M_1 metamorphism

The most prominent feature of D_1 deformation is a well developed cleavage (S_1) seen throughout the southern SRR (Fig. 4a). S_1 is a penetrative, slaty to phyllitic foliation in metapelite (Fig. 5a), and a closely-spaced cleavage in metasiltstone and thin-bedded quartzite. A flaggy, spaced cleavage is locally developed in some thicker quartzite beds (Fig. 5b); however, many of these beds lack any evident fabric. The cleavage strikes NE and dips, on average, steeply to the NW (Fig. 4b), reflecting NW–SE shortening. It is commonly subparallel to bedding (Fig. 4b) because associated D_1 folds of bedding are tight to isoclinal, but it is demonstrably axial planar to these folds where hinge regions are exposed (see Section 3.2).

In thin sections of slates and phyllites, the S_1 foliation is a continuous cleavage defined by the grain shape-alignment of abundant fine-grained white mica and less common chlorite, elongate quartz grains with minute pressure shadow beards, and seams of opaque material (Fig. 6a). In metasiltstones, the S_1 cleavage is closely-spaced rather than continuous, and defined primarily by seams of opaque material in cleavage domains, and long axes of quartz grains in microlithon domains, in addition to grain-shape alignment of minor metamorphic white mica and chlorite (Fig. 6b). Evidence that pressure solution was the primary process involved in S_1 cleavage formation in these rocks includes the following features (Fig. 6b; Knipe, 1981; Borradaile et al., 1982; Ho et al., 1995). (1) Evidence for dissolution and reprecipitation of quartz: elongate quartz grains in microlithon domains have relatively flat top and bottom surfaces next to adjacent cleavage domains, and well-developed pressure shadow beards in the plane of cleavage. (2) Evidence for residual accumulation of less-dissolvable materials: opaque material and detrital muscovite are most abundant in cleavage domains.

Much less evidence for strain is found in quartzites, many

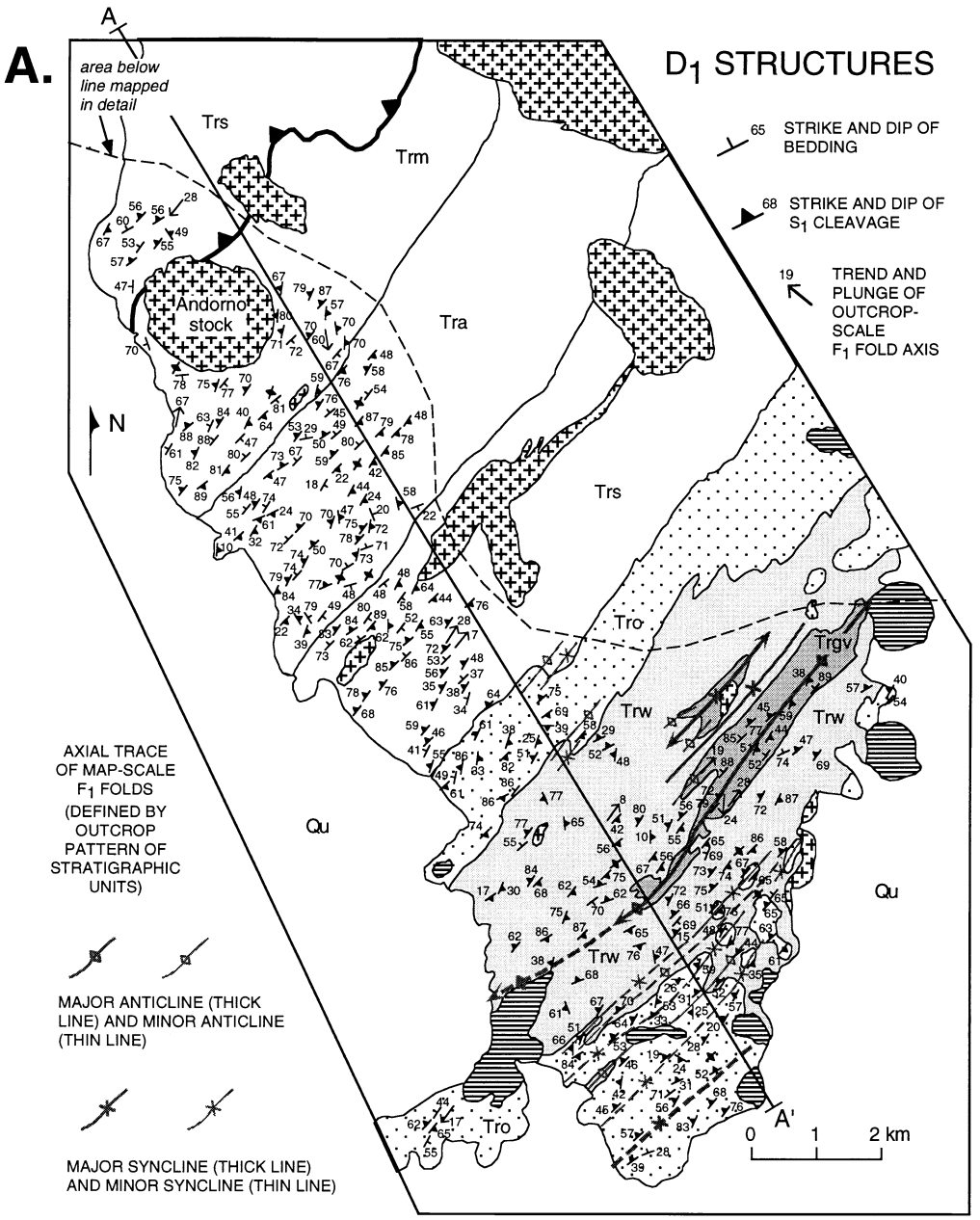
A.
A
A'
area below line mapped in detail
D1 STRUCTURES
65 STRIKE AND DIP OF BEDDING
68 STRIKE AND DIP OF S1 CLEAVAGE
19 TREND AND PLUNGE OF OUTCROP-SCALE F1 FOLD AXIS
Andorno stock
Trs
Trm
Tra
Tro
Trw
Trgv
Qu
N
AXIAL TRACE OF MAP-SCALE F1 FOLDS (DEFINED BY OUTCROP PATTERN OF STRATIGRAPHIC UNITS)
MAJOR ANTICLINE (THICK LINE) AND MINOR ANTICLINE (THIN LINE)
MAJOR SYNCLINE (THICK LINE) AND MINOR SYNCLINE (THIN LINE)
0 1 2 km

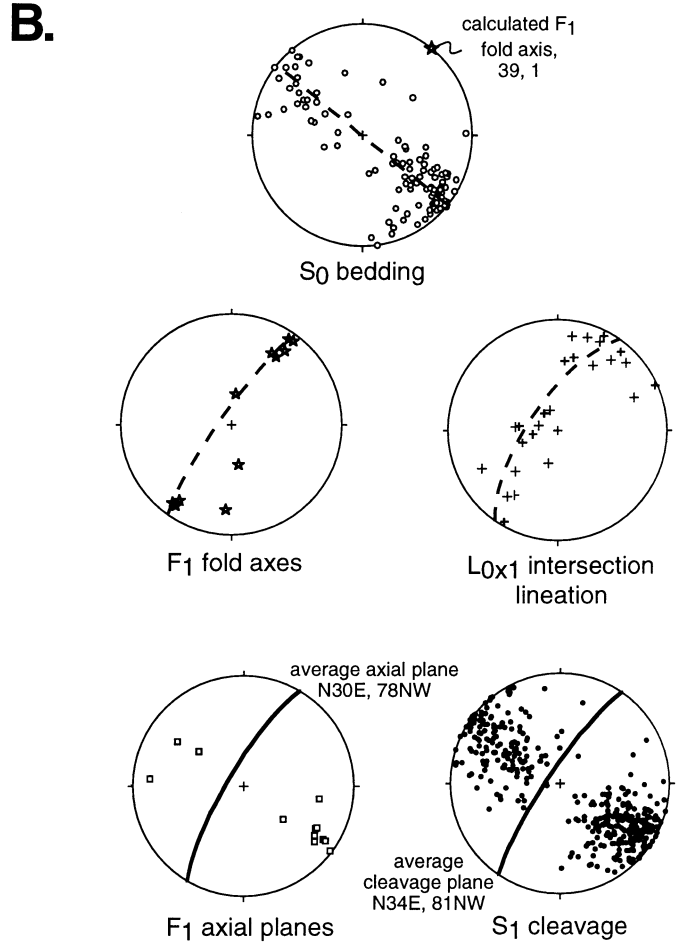
B.
calculated F1 fold axis, 39, 1
S0 bedding
F1 fold axes
L0x1 intersection lineation
average axial plane N30E, 78NW
F1 axial planes
average cleavage plane N34E, 81NW
S1 cleavage

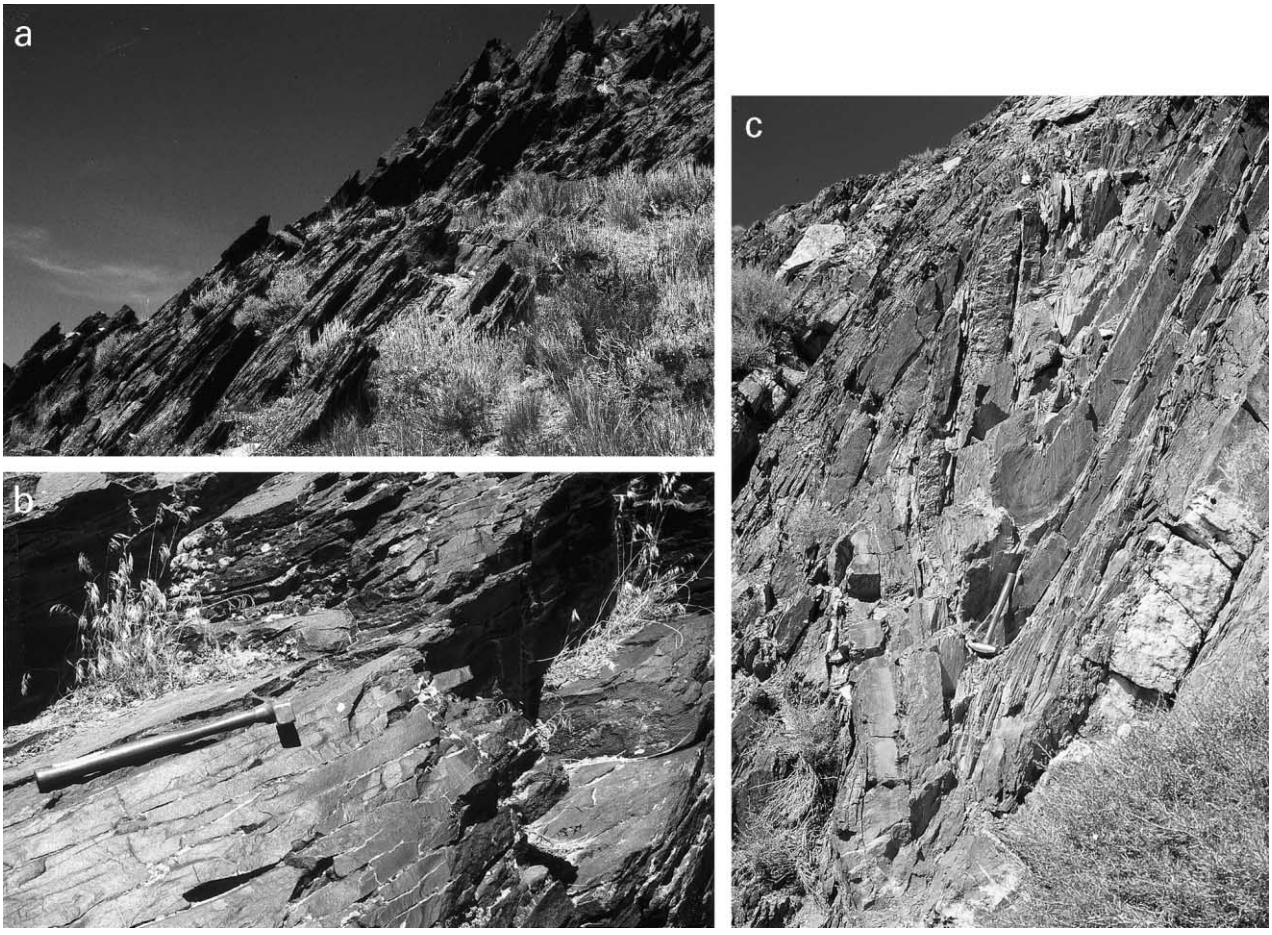

Fig. 5. (A) Typical continuous, slaty to phyllitic S_1 cleavage in Singas Formation metapelites in central part of study area. View to northeast. Shrubs for scale are about 30 cm tall. (B) Typical spaced S_1 cleavage in quartzite of O'Neill Formation. View to north. Hammer handle for scale is 32 cm long. (C) View to northeast of F_1 fold in interbedded quartzite and slate of O'Neill Formation. Note axial planar S_1 cleavage; tight, similar shape; axial plane dipping steeply to northwest; and asymmetry with vergence to southeast. S_1 cleavage most evident in slate but also present in inner hinges of quartzite beds. Hammer handle for scale is 35 cm long.

of which do not contain a well-developed fabric (Fig. 6c). Where present, the S_1 cleavage is spaced, only weakly to moderately developed, and defined by discontinuous seams of opaque material, grain shape alignment of minor metamorphic white mica and chlorite, quartz grains that are locally slightly elongate, and poorly-developed pressure shadow beards at the ends of some quartz grains. Quartz grains typically have undulose extinction, but show only minor development of subgrains related to recovery processes or small strain-free neocrystals related to dynamic recrystallization (Fig. 6c). Collectively, these features indicate that crystal-plastic deformation processes were of limited importance in D_1 strain of these rocks, consistent with the low grade of M_1 metamorphism (Passchier and Trouw, 1996; Rogers, 1999).

3.2. F_1 folds

F_1 folds in Triassic strata of the southern SRR range from tens of centimeters to a few meters in wavelength to many kilometers in wavelength. Characteristic features of these folds are: tight to isoclinal limb appression; fold axes that plunge shallowly to the NE and SW; axial planes that are, on average, NE-striking and steeply-dipping and parallel to the S_1 cleavage; and commonly asymmetric limb dip and length, indicating vergence and overturning to the southeast.

Outcrop-scale F_1 folds are evident only in exposures of quartzite or interlayered quartzite and slate. These folds fold bedding and have an axial planar S_1 cleavage (Fig. 5c). Outcrop-scale F_1 folds are not generally seen in exposures dominated by slate, presumably due to the lack of any

Fig. 4. (A) Map of southern Santa Rosa Range showing contacts, and orientation of bedding and D_1 structures from area of detailed study. Patterns and unit symbols the same as in Fig. 3. (B) Lower-hemisphere equal-area projections of orientation data for D_1 structures. Open circles are poles to bedding planes (best-fit great circle and calculated F_1 fold axis shown); stars are measured F_1 fold axes; crosses are intersection lineations between bedding and S_1 foliation; open boxes are poles to F_1 axial planes (average axial plane orientation shown); solid dots are poles to S_1 cleavage planes (average cleavage plane orientation shown).

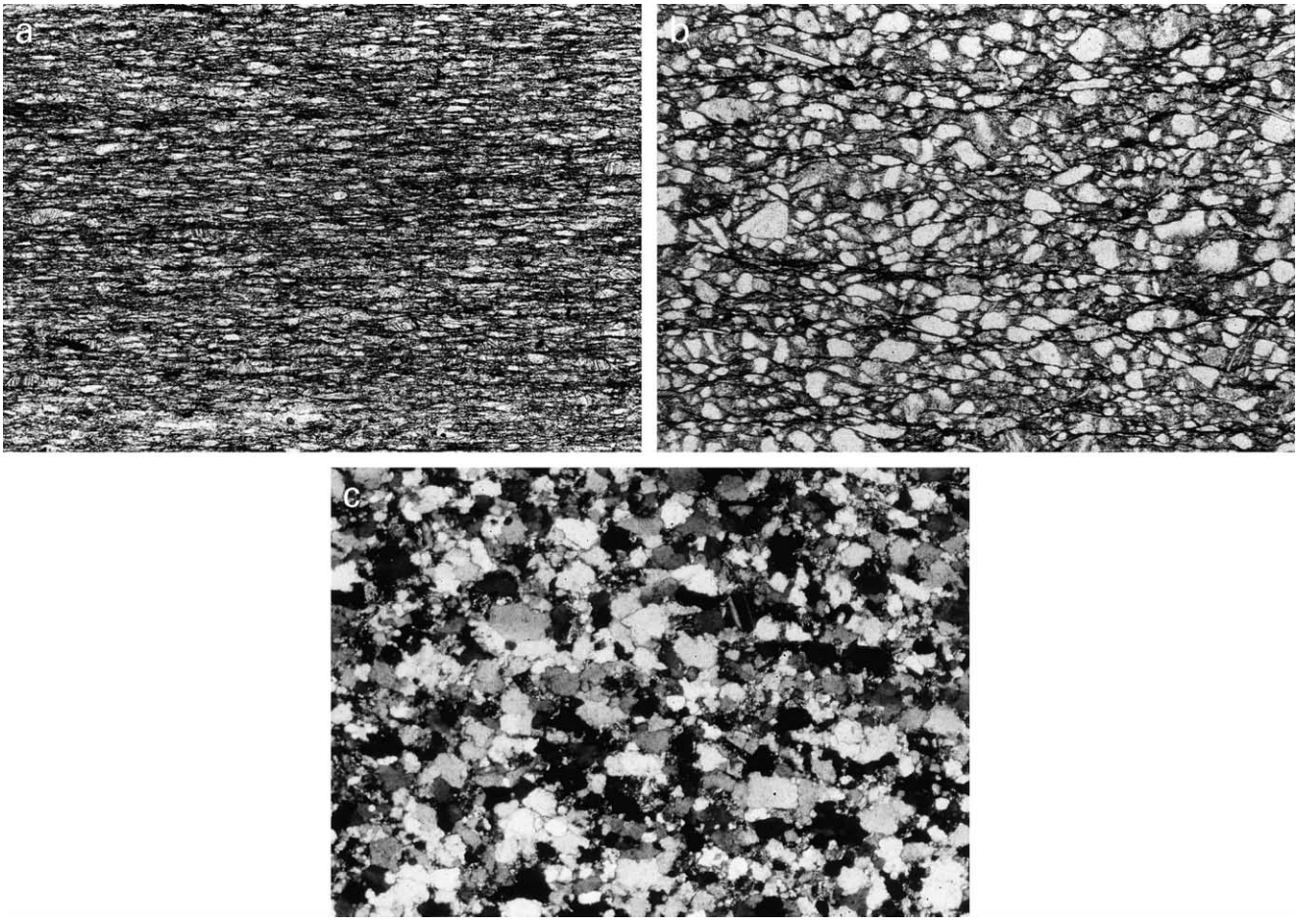

Fig. 6. (A) Photomicrograph (plain light) of typical S_1 cleavage in metapelite from Singas Formation in the central part of the study area. Long dimension is 1.3 mm. S_1 (horizontal) defined by cleavage domains of aligned white mica and chlorite (thin grey crystals) and opaque material (black), and microlithons of elongate quartz grains (white). (B) Photomicrograph (plain light) of typical S_1 cleavage in silty quartzite of O'Neill Formation. Long dimension is 3.2 mm. S_1 (horizontal) defined by cleavage domains rich in opaque material (black), and microlithons containing slightly elongate quartz grains (white) with well-developed pressure shadows (grey). (C) Photomicrograph (cross-nicols) of typical S_1 spaced cleavage in quartzite from Andorno Formation. Long dimension is 3.2 mm. Weak S_1 (horizontal) defined by slightly elongate quartz grains.

marker horizons. In F_1 folds of interlayered quartzite and slate, the slate beds form class 2 similar folds with a pervasive S_1 cleavage and significantly thickened hinges and thinned limbs, whereas the quartzite beds are generally cleaved only in the hinge area and typically form class 1B parallel or class 1C folds with slightly thickened hinges (Fig. 5c).

Fold axes of the outcrop-scale F_1 folds plunge shallowly to moderately to the NE and SW, based on measured axes of folds and the fold axis calculated from the girdle distribution of folded bedding poles (Fig. 4b). $L_{0\times1}$ (bedding-S_1) intersection lineations are of similar orientation to F_1 fold axes (Fig. 4b), consistent with the fact that the S_1 cleavage is axial planar to the F_1 folds (Fig. 5c). Axial planes of the outcrop-scale F_1 folds strike NE and dip steeply to the NW or SE, with the majority of measured axial planes dipping to the NW (Fig. 4b). The calculated average axial plane orientation of N30E, 78NW is subparallel to the average great circle girdle distribution of F_1 fold axis and $L_{0\times1}$ data. This relation is expected in non-cylindrical folding, and provides evidence for two conclusions. First, scatter in the orientation of F_1 fold axes and $L_{0\times1}$ lineations primarily reflects non-cylindrical F_1 folding, not reorientation of the D_1 structures by later deformation. Second, the steeply NW-dipping average axial plane orientation shown in Fig. 4b is representative of the F_1 axial plane orientation. The geometry of the outcrop-scale F_1 folds indicate that they reflect NW–SE shortening and structural transport to the SE (top-to-the-SE shear).

Map-scale folds are manifested in the southern SRR by the outcrop pattern of the O'Neill (Tro), Winnemucca (Trw), and Grass Valley (Trgv) Formations in the southeast part of the area (Fig. 4a). A major anticline bisects the larger area of exposure of unit Trgv and a major syncline bisects the southeastern part of unit Tro. Several smaller folds defined by the map-pattern of the Triassic units are also evident in this area (Fig. 4a). All of these folds have NE-trending axial traces, with hinge lines that plunge variably to

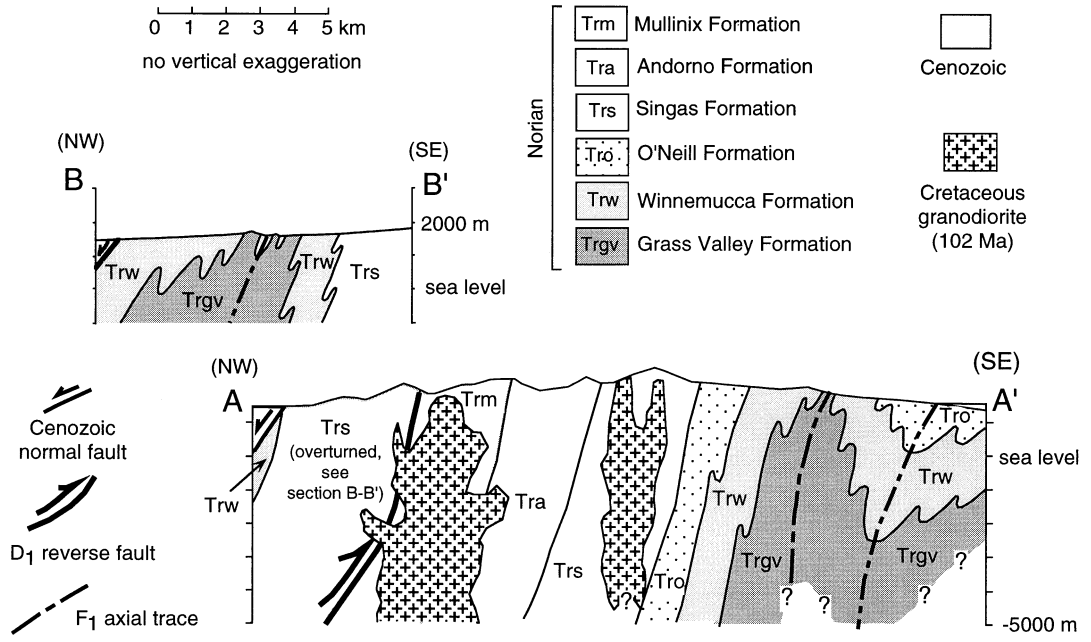

Fig. 7. Structure sections A–A′, from southern Santa Rosa Range, and B–B′, from northern Santa Rosa Range; see Figs. 3 and 4 for location of section lines. Section A–A′ drawn from area of detailed mapping (Rogers, 1999). Section B–B′ based on data of Compton (1960) and does not show local topography; section drawn to illustrate relations in hanging wall of reverse fault transecting Santa Rosa Range (Fig. 3).

the NE and SW. The overall map pattern is one that indicates: (a) large-scale folding of units into a major anticline and major syncline, with superimposed parasitic folding on the major fold limbs and, especially, within the major fold hinge areas; and (b) asymmetry to the major folding, with vergence to the southeast. This pattern is shown in the structure-section of Fig. 7.

The size of the map-scale F_1 folds is quite large, with wavelengths of several kilometers (Figs. 4 and 7). Units Trs, Tra and Trm form the long western limb of the major map-scale F_1 anticline, and this limb is cut to the west by the reverse fault that bisects the SRR (Figs. 4 and 7). Compton's (1960) mapping to the north of our study area suggests that additional map-scale F_1 folding is present west of this reverse fault (Fig. 3). Specifically, his mapping and structural data indicate that the Grass Valley and Winnemucca Formations in the northwest SRR form the core of a major NE–SW trending anticlinal structure that is affected by considerable smaller scale (parasitic?) folding within the hinge region, and that the Singas Formation just west of the reverse fault forms the overturned eastern limb of this major anticline. These relations are shown schematically in cross-section B–B′ in Fig. 7, which is based on the structural and map data of Compton (1960), ignoring local topography.

3.3. D_1 faulting

Compton (1960) mapped a reverse fault that repeats the Triassic stratigraphy in the western SRR (Fig. 3). Our mapping in the southern SRR confirms the existence of this fault, based on the juxtaposition of the Singas Formation on top of the younger Mullinix Formation (Fig. 4a). This fault clearly predates emplacement of Cretaceous intrusions, several of which cut directly across the fault (Figs. 3 and 4).

In the southern SRR (Fig. 4a), the fault trends NE and has a subvertical to steep NW dip (Rogers, 1999). The orientation of the fault changes along strike, however, suggesting that it has been reoriented by some younger process, probably deflection during emplacement of the Cretaceous intrusions that cross-cut it (Rogers, 1999; Fig. 3). Detailed study of structural relations along the fault is made difficult by the fact that it occurs almost entirely within the metamorphic aureoles of Cretaceous intrusions, where younger metamorphism significantly obscures the character of older structures (see Section 6). Nonetheless, it appears most likely that the fault developed during D_1 deformation, based on the following. (1) The fault is oriented subparallel to the S_1 cleavage and to the axial planes of F_1 folds (Figs. 4 and 7). This is consistent with a conclusion that faulting, S_1 cleavage development, and F_1 folding were all related responses to the same strain regime. (2) There is no evidence to support a conclusion that the fault formed during any of the younger phases of deformation in the southern SRR, because the younger phases either clearly cross-cut the fault, reflect a very different shortening direction, and/or reflect too little strain to be consistent with large-scale faulting. (3) Development of this fault during D_1 deformation is consistent with regional relations, indicating that similar reverse faulting accompanied the first phase of deformation elsewhere in the LFTB (see Section 7).

3.4. Summary, kinematics and total shortening during D_1

The data discussed above indicate that D_1 deformation in the southern SRR involved tight to isoclinal, megascopic and mesoscopic folding of bedding, development of a regional cleavage, and reverse faulting. Orientation of these structures indicates that the shortening direction during D_1 deformation was NW–SE. Asymmetry of folds indicate that tectonic transport was to the southeast. This is consistent with the northwest dip of the D_1 reverse fault.

The amount of shortening affecting the southern SRR during D_1 deformation can be estimated based on shortening values associated with folding. To do this, we measured the initial length (along beds) between two points in layers folded by outcrop-scale D_1 folds, and the final horizontal distance between these two points, and then calculated percent shortening. These measurements all indicate 55–72% shortening. This does not take into account shortening associated with development of the regional S_1 cleavage or shortening associated with the D_1 reverse fault. We therefore conclude that shortening associated with D_1 deformation was in excess of 55–70%.

3.5. Age constraints for D_1 deformation

D_1 deformation in the southern SRR has been dated by whole-rock $^{40}Ar/^{39}Ar$ analyses of slates and phyllites (Wyld et al., 1999). These data, details of which will be presented elsewhere, indicate that D_1 deformation and syntectonic M_1 metamorphism in the southern SRR occurred prior to a minimum age of ~140 Ma, and most likely occurred significantly prior to this minimum age. Farther south in the LFTB, in the west Humboldt Range (Fig. 2), identical D_1 structures predate intrusion of a pluton dated at 165 Ma (U–Pb zircon analysis; Wyld and Wright, 2000). Farther west in the northern LFTB, in the Jungo area (Fig. 2), identical D_1 structures likely formed simultaneously with deformation between 201 and 193 Ma in arc rocks of the Jackson Mountains (Quinn et al., 1997; Folsom, 2000; Wyld and Wright, 2000). A final age constraint is that D_1 deformation must postdate deposition of the youngest deformed units. In the SRR, these strata are latest Triassic age (Lupe and Silberling, 1985). In the west Humboldt Range, the youngest strata deformed by D_1 deformation are early Toarcian (late Early Jurassic; Speed, 1974). In summary, data from the SRR indicate that D_1 deformation occurred in the Jurassic, and regional relations elsewhere in the northern LFTB require more specifically that it occurred sometime in the late Early and/or early Middle Jurassic.

4. D_2 deformation

D_2 deformation produced structures reflecting heterogeneous strain in the southern SRR. D_2 is most pronounced in the southeastern part of the SRR, in the Grass Valley, Winnemucca, and O'Neill Formations, where structures include F_2 folds and an associated S_2 cleavage (Fig. 8a). Farther northwest, in the Singas, Andorno and Mullinix Formations, D_2 is manifested by a weakly-developed, heterogeneously-distributed, kink-band fabric (S_{2k}; Fig. 8a). Although the character of structures vary from southeast to northwest, they are interpreted to be related, as explained below.

4.1. D_2 folds and S_2 cleavage in the southeast

In the southeastern part of the study area, D_2 structures are found locally in all rock types (quartzite, metasiltstone, and slate). These structures include mesoscopic F_2 folds of bedding and the S_1 cleavage, and a spaced S_2 cleavage that cuts S_1.

Outcrop-scale F_2 folds have an open to close, class 1B shape (Fig. 9), and are clearly distinguishable from F_1 folds because they fold the S_1 foliation, they are more open and more parallel, and they are associated with only limited development of an axial planar cleavage, even in slates (Fig. 9). Megascopic F_2 folds in the southeastern SRR are widespread, as manifested by the varying orientation of S_1 cleavage (Figs. 4a and 8a). These folds are discontinuous along their axial trace and appear to be relatively homogeneously distributed in the southeastern SRR, with no obvious major antiforms or synforms (Fig. 8a). F_2 folds, both mesoscopic and megascopic, are most abundant in the Grass Valley and Winnemucca Formations, and in the southeasternmost exposures of the O'Neill Formation (Fig. 8a).

The S_2 cleavage is spaced (Fig. 9), and developed by pressure solution with no evident associated growth of metamorphic minerals. It is present in two settings. (1) In the hinge region of outcrop-scale F_2 folds (Fig. 9a and c). Here it is axial planar to the F_2 folds and it clearly cross-cuts the folded S_1 foliation. There is usually no S_2 cleavage developed on the limbs of F_2 folds. (2) S_2 is also locally present in areas without any evident outcrop-scale F_2 folds. In this setting, S_2 cleavage is recognized by the fact that it cross-cuts the S_1 cleavage.

The orientation of F_2 folds and S_2 cleavage is shown in Fig. 8b. F_2 axial planes and the S_2 cleavage both strike northeast and dip, on average, steeply to the northwest. Measured outcrop-scale F_2 fold axes are subhorizontal and trend NE and SW, consistent with the F_2 fold axis calculated from the distribution of S_1 foliation poles in the southeastern SRR. This is nearly identical to the orientation of $L_{1\times2}$ (S_1 and S_2) intersection lineations, consistent with the field evidence that the S_2 cleavage is axial planar to the F_2 folds. The fairly tight cluster in orientations of F_2 fold axes and $L_{1\times2}$ intersection lineations indicates that the F_2 folds are relatively cylindrical in shape, consistent with field observations.

Because the F_2 folds in the southern SRR are most prominent in the area where map-scale folds of stratigraphic units are also prominent, and because both F_1 and F_2 folds

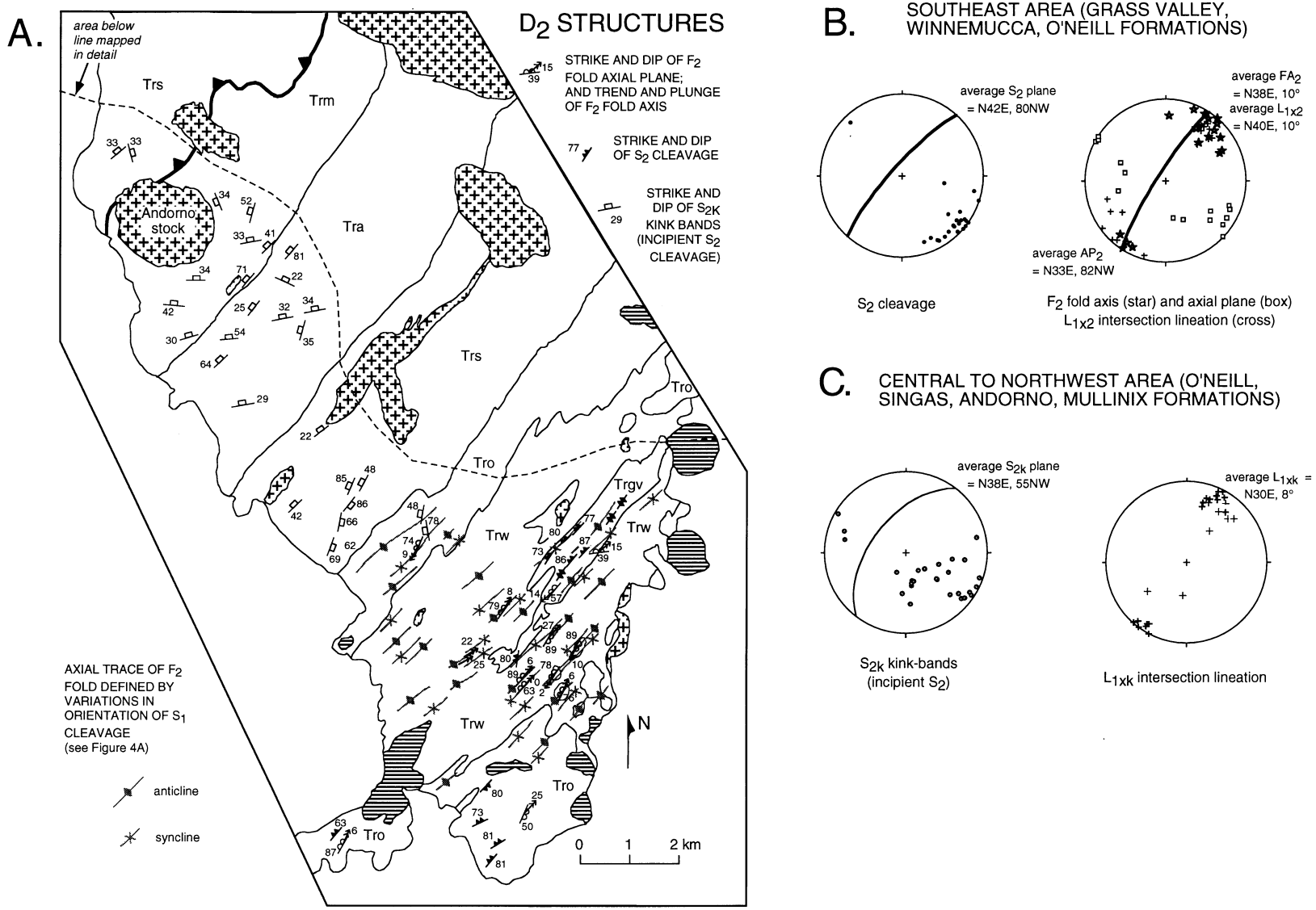

Fig. 8. (A) Map of southern Santa Rosa Range, showing location and orientation of D_2 structures. Triassic units not patterned to make structural symbols more evident; otherwise, patterns and unit symbols same as in Fig. 3. (B and C) Lower-hemisphere equal-area projections of orientation data for D_2 structures. Open boxes are poles to F_2 axial planes; stars are F_2 fold axes; black dots are poles to S_2 cleavage; grey dots are poles to S_{2k} kink band fabric; crosses are intersection lineations between S_1 and S_2 or S_{2k} cleavages. (B) Data from southeast part of range where D_2 is manifested by folds and a spaced S_2 cleavage. (C) Data from northwest part of range where D_2 is manifested by S_{2k} kink band fabric.

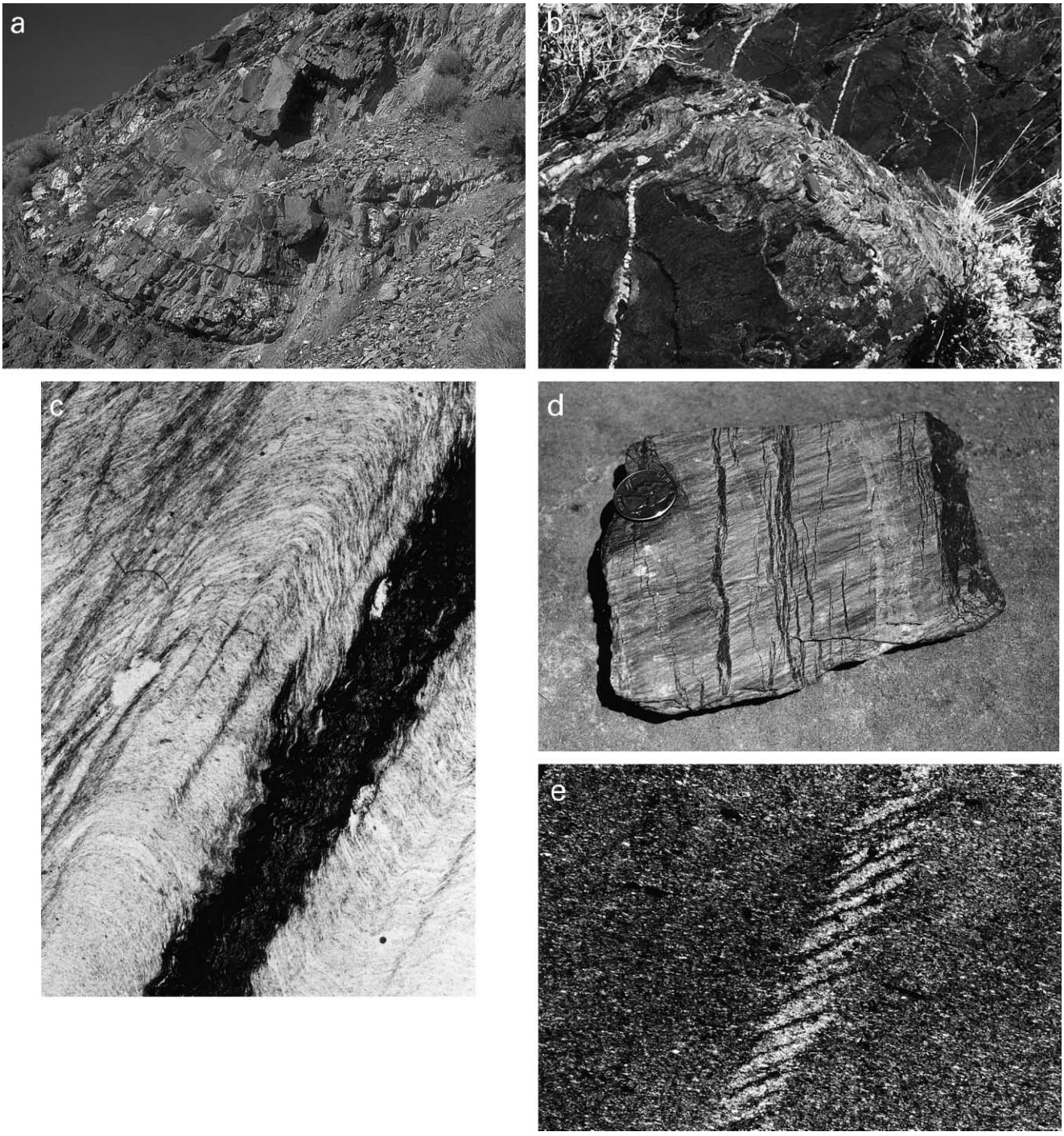

Fig. 9. (A) View to north of F_2 folds in interbedded quartzite and slate of O'Neill Formation. Note gentle, parallel shape, and steeply-dipping, spaced, axial-planar cleavage (S_2). S_1 cleavage is parallel to bedding and visible only in slates in lower left of photo. Bushes for scale are about 30 cm tall. (B) View to southwest of F_2 folds of spaced S_1 cleavage in quartzite of O'Neill Formation. Note gentle to open, parallel shape, and lack of any axial planar cleavage. Knife for scale is 9 cm long. (C) Photomicrograph (plain light) of polydeformed slate from Winnemucca Formation. Long dimension is 6.5 mm. S_1, defined by aligned white mica, is folded about F_2 fold whose axial trace trends from lower left to upper right. Spaced S_2 cleavage is parallel to F_2 axial trace, and rich in mica and opaque material. D_4 crenulation folds are evident in wide S_2 cleavage domain (dark band) and have axial traces that trend from upper left to lower right. Note that D_4 crenulations clearly cross-cut S_2 cleavage. (D) S_{2k} kink bands cutting S_1 cleavage in slate of Singas Formation from central part of study area. Coin for scale is about 2.4 cm in diameter. S_1 cleavage, defined primarily by aligned M_1 white mica, is parallel to surface face of rock (light gray). S_{2k} kink bands are irregularly spaced, anastomosing, and discontinuous dark bands that cut across rock from top to base of photo. M_1 white mica is realigned in kink bands so that it dips to right. Oblique face on right side of rock has preferentially broken parallel to kink-band fabric. Wavy aspect on surface face of rock is caused by D_4 crenulations, which cut and crenulate the S_{2k} fabric. (E) Photomicrograph (cross-nicols) of kink-band fabric in Singas Formation slate from central part of study area. Long dimension is 3.2 mm. S_1 cleavage trends from 280 to 100°. Single kink band trends across center of photo, and reorients S_1 mica and chlorite, creating a light-colored optical discontinuity. Spaced D_4 crenulation cleavage, defined by dark bands, cross-cuts kink band from lower left to upper right.

have similarly-oriented fold axes and axial planes (Figs. 4 and 8), it is important to explain why we interpreted the map-scale folding of stratigraphic units in the southeast part of the study area to be related to D_1, not D_2, deformation. The reasons for this conclusion are as follows.

1. Outcrop-scale F_1 folds are tight to isoclinal, and asymmetric with vergence to the southeast (Fig. 5c), which is consistent with the geometry of the map-scale folds of stratigraphic units in the southeastern SRR (Figs. 4 and 7). In contrast, outcrop-scale F_2 folds are generally open and do not exhibit any evident consistent sense of asymmetry (Fig. 9), which does not match the geometry of the map-scale folds.
2. Outcrop-scale F_1 folds have fold axes that plunge variably to the SW and NE, consistent with the geometry of the map-scale folds of stratigraphic units (Fig. 4); whereas outcrop-scale F_2 folds have relatively tightly clustered subhorizontal axes (Fig. 8b) that would be less likely to produce the map pattern of the folded units.
3. If the map-scale folds of stratigraphic units were developed during D_2 deformation, then the folds would fold both stratigraphic layering and the S_1 foliation in the same manner. If this was the case, anticlines and synclines defined by the map pattern of the stratigraphic units should be associated with anticlines and synclines, respectively, defined by varying orientations of S_1 foliation. This is not the case, however. While the S_1 foliation clearly varies in orientation in the southeastern SRR due to later deformation (Fig. 4b), the folds that fold S_1 do not correspond well with folds defined by the map-pattern of stratigraphic units. In some cases, where the map-pattern of the Triassic units define a fold of one geometry (e.g. an anticline), the varying orientation of S_1 cleavage in the same area defines a fold of the opposite geometry (i.e. a syncline) (Fig. 4a). It is thus clear that two phases of folding have affected units in the southeastern SRR, not just one.

Based on the evidence noted above, we conclude that the map pattern of units Tro, Trw and Trgv in the southeastern SRR is primarily a result of F_1 folding. It also appears, however, that later F_2 folding in this same area influenced the final shape of these major F_1 folds. This conclusion is based on the observation that the only place where the S_2 cleavage is widespread and not associated with any evident outcrop-scale F_2 folds, is in the hinge regions of the major F_1 folds — i.e. in the Grass Valley Formation in the hinge region of the major F_1 anticline, and in the southeasternmost exposures of the O'Neill Formation in the hinge region of the major F_1 syncline (Fig. 8a). Because most F_2 folds show only limited development of an axial planar S_2 cleavage (see Fig. 9), the more widespread development of S_2 in the hinge regions of F_1 folds suggests that these were areas of higher D_2 strain. We therefore suggest that D_2 deformation in the southeastern SRR resulted not only in F_2 folding, but also in tightening of prior F_1 folds in this area.

4.2. D_2 kink-band fabric in the northwest

Moving to the northwest, into the northwest part of the O'Neill Formation, F_2 folds decrease in abundance and the spaced S_2 cleavage is replaced by a weakly-developed and heterogeneously-distributed kink-band fabric that cuts the S_1 foliation. Farther west, in the Singas, Andorno, and Mullinix Formations, F_2 folds are absent, and the only D_2 structure present is the kink-band fabric (Fig. 8a). The kink-band fabric is only present in slates and phyllites, never in sandstones, and is manifested in outcrop as wavy, discontinuous zones in which the S_1 foliation has a different orientation from S_1 in the rest of the rock (Fig. 9d). Thin section petrography indicates that the kink bands reorient the metamorphic muscovite defining the S_1 foliation, thus creating an optical discontinuity (Fig. 9e). There is no petrographic evidence for metamorphic mineral growth during development of the kink bands.

Kink-band structures show a similar orientation to D_2 structures farther southeast (Fig. 8c). Like S_2 and the axial planes of F_2 folds, the kink bands strike NE and dip, on average, steeply to the NW. Like $L_{1\times2}$, the intersection lineation between S_1 and the kink band fabric ($L_{1\times k}$) forms a subhorizontal, NE to SW trending cluster. Although of similar orientation to D_2 structures farther southeast, the kink-band fabric clearly reflects much lower strain and much less shortening than the F_2 folds and S_2 cleavage.

The following relations support a conclusion that the F_2 folds and S_2 spaced cleavage in the southeastern part of the study area are related to the kink-band fabric seen farther to the northwest. First, the structures have very similar orientations and reflect a similar NW–SE shortening direction (Fig. 8b). Second, the folds and the spaced cleavage die out in the general area where the kink-band fabric appears (in the O'Neill Formation in the central part of the map area; Fig. 8a). Third, there is a consistent pattern of decreasing strain represented by these structures from southeast to northwest across the southern SRR. Fourth, the folds, spaced cleavage and kink-band fabric all post-date the S_1 foliation (Fig. 9), and predate D_3 and D_4 structures (see Sections 5 and 6). Based on these relations, the kink-band fabric is interpreted to be an incipient, weakly-developed manifestation of the S_2 spaced cleavage, and D_2 strain is interpreted to weaken to the northwest in the southern SRR. Initial stages of cleavage development in slates and phyllites typically involve kinking and folding of phyllosilicate minerals (White and Knipe, 1978), so that this interpretation appears reasonable for the kink-band fabric.

4.3. Summary, interpretation and total shortening during D_2

D_2 deformation in the southern SRR produced open to close, parallel F_2 folds and an axial-planar, spaced cleavage (S_2) in the southeast part of the study area, and a weakly-developed

kink-band fabric to the northwest. These structures reflect shortening in a NW–SE direction, with increasing strain toward the southeast.

Any interpretation of D_2 deformation in the southern SRR must include an explanation for the D_2 strain gradient across the area. A plausible explanation for this feature builds on the concept that strain typically increases in some fashion toward syntectonic faults (Ramsay and Huber, 1987). This suggests that D_2 strain may increase toward the southeast because a D_2 fault is located in this direction, presumably buried to the east under Quaternary alluvium (Figs. 3 and 4). Support for this interpretation comes from structural studies elsewhere in the northern LFTB, as discussed further in Section 7.

Shortening associated with D_2 structures can be estimated by considering initial and final length measurements in F_2 folds and kink bands. Based on this type of analysis, folding to the southeast accommodated up to about 15–20% shortening, while the kink-bands to the northwest accommodated about 2–3% shortening. These estimates are considered a maximum because D_2 structures are only locally developed and are not pervasive in areas where they occur. Total shortening associated with D_2 deformation in the southern SRR is therefore much less than that associated with D_1.

4.4. Age constraints for D_2 deformation

The timing of D_2 deformation in the southern SRR is loosely constrained to the Jurassic and/or Early Cretaceous, based on the fact that D_2 structures postdate the Early to Middle Jurassic D_1 deformation, and predate deformation associated with intrusion of mid-Cretaceous plutons (see Section 6). Regional relations, discussed in Section 7, provide additional insight into the timing of D_2 deformation and suggest that it occurred sometime in the Middle to Late Jurassic interval.

5. D_3 deformation

D_3 deformation produced large open folds of the older cleavages. These F_3 folds are distinctive from other fold phases because they are large, with wavelengths of tens of meters; gentle to open in shape; and have subhorizontal axial planes (Fig. 10a). They are manifested by hillside-scale variations in the dip direction (SE versus NW) of the S_1 foliation, with areas of NW- versus SE-dipping S_1 separated by areas in which the S_1 foliation is near vertical (Figs. 4a and 12a). These folds are most obvious in the central to western part of the study area, and are particularly evident in the Andorno Formation.

F_3 folds have subhorizontal, NE-trending fold axes, based on folding of S_1 within the Andorno Formation (Fig. 10b). This is quite similar to the orientation of F_2 fold axes in the southeastern SRR (Fig. 8b), and indicates that care must be exercised when trying to resolve the effects of the F_2 versus the F_3 phases of folding. Our observations in the southern SRR indicate that D_2 strain decreases significantly from southeast to northwest, and that D_2 outcrop-scale folds decrease in abundance from southeast to northwest and are absent northwest of the O'Neill Formation (Fig. 8a). Therefore, we conclude that the effects of F_2 folding are negligible in the Singas, Andorno, and Mullinix Formations, and that S_1 foliation orientations from these three units provides the clearest information on the geometry of F_3 folding.

Stereonet plots of S_1 foliation poles from the Singas, Andorno, and Mullinix Formations are shown in Fig. 10c. The pole data define an F_3 fold axis that is NE-trending and subhorizontal. In addition, two clusters of pole data are seen, one reflecting an average plane dipping 78°NW, the other reflecting an average plane dipping 43°SE. This pattern is consistent with the geometry of observed hillside-scale F_3 fold limbs (Fig. 10a). The axial plane calculated as the gently-dipping bisector of these average fold limbs dips 18°NW. This is consistent with the geometry of observed hillside-scale F_3 folds, whose axial planes are subhorizontal (Fig. 10a).

Field and stereonet evidence for the orientations of F_3 axial planes indicates that D_3 shortening was in a subvertical direction. There is no compelling evidence that D_3 deformation involved a component of simple shear. This is because F_3 folds appear symmetric where fold trains are visible, and because the structural data that provides evidence for two oppositely-dipping F_3 fold limb orientations does not indicate a greater abundance of one limb orientation relative to the other (Fig. 10b and c), which would be expected if the folds were asymmetric. The strain associated with D_3 is thus interpreted to be broadly pure-shear with subvertical shortening and subhorizontal extension.

Fig. 10d also shows stereonet data for S_2 cleavages. The S_{2k} kink-band fabric in the Mullinix, Andorno, Singas, and western part of the O'Neill Formation is folded about a NE-trending, subhorizontal fold axis, similar to the F_3 fold axis defined by folded S_1 foliation in the same area. The S_2 spaced cleavage from the southeastern part of the study area, however, is not significantly folded. This suggests that F_3 folding had little impact in the southeastern part of the study area.

D_3 deformation represents a very low strain event with only minor associated shortening; values determined from bed-length measurements on photographs of F_3 folds in the Andorno Formation indicate that they accommodated 4–5% shortening. D_3 deformation is also heterogeneously distributed in the southern SRR, having had little impact on the southeastern part of the study area. This indicates that the shortening value determined from folds in the Andorno Formation should be considered a maximum. The relative timing of D_3 deformation is defined by the following. S_1 foliation and the S_{2k} kink-band fabric are both folded by the F_3 folds (Fig. 10b–d), and F_3 folds therefore

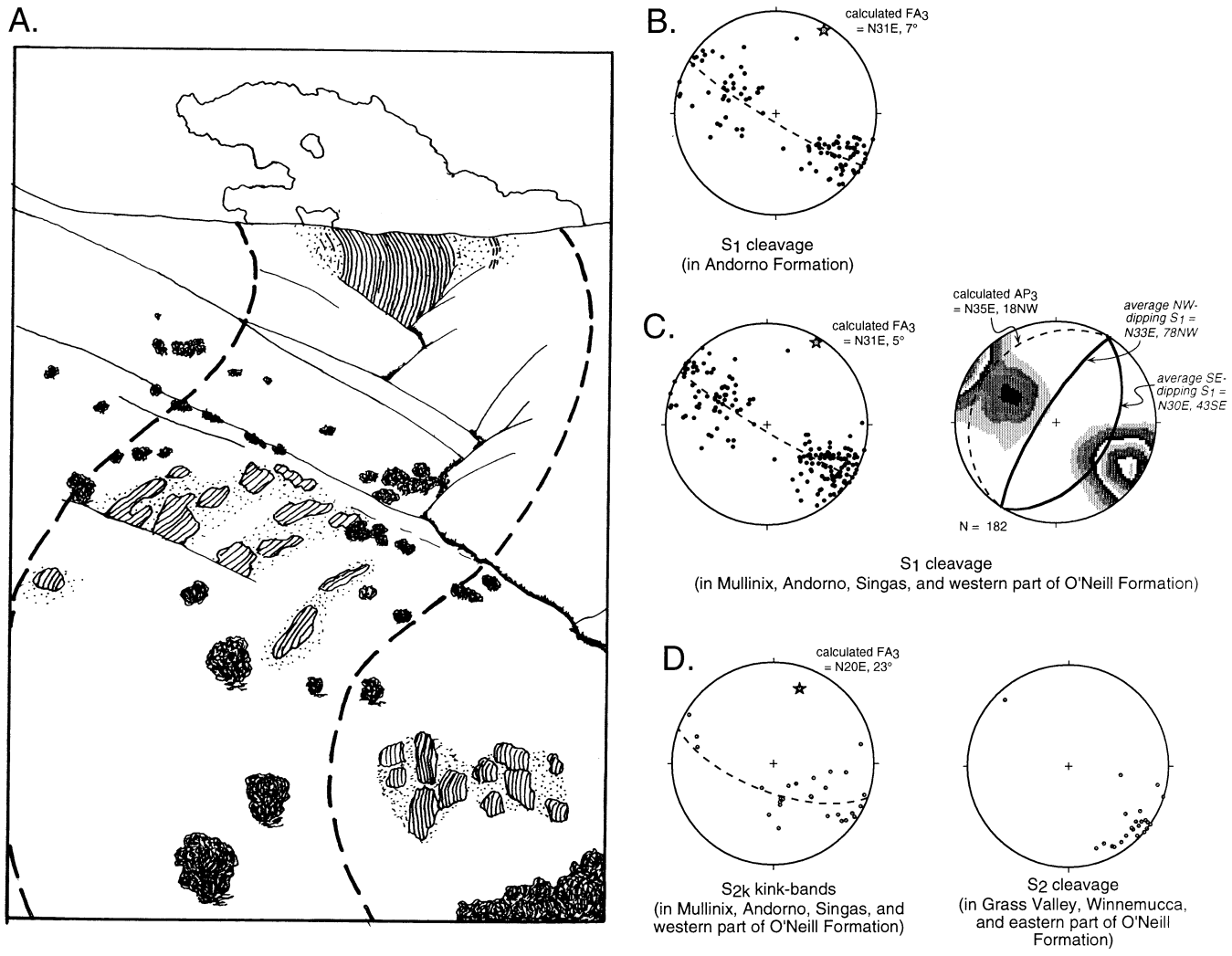

Fig. 10. (A) Sketch of a photograph showing D_3 folds of S_1 cleavage in Andorno Formation slates, looking to northeast up a valley toward skyline. Horizontal and vertical distance from front (base) of photo to back (skyline) is about 1300 and 500 m, respectively. Dark patches are sagebrush shrubs. Striped areas are outcrops, and stripes show orientation of S_1 cleavage, which forms a prominent and visible fabric in slates. Dots are areas of rocky ground around outcrops. Thick dashed lines are drawn to show overall shape of folds. Note subhorizontal axial trace and open, rounded shape of folds. (B–D) Lower-hemisphere equal-area projections of structural data yielding information on D_3 folding. (B) Poles to S_1 cleavage in Andorno Formation. F_3 fold axis calculated from great circle defined by poles to S_1 cleavage. (C) Poles to S_1 cleavage, plotted as scatter and Kamb contour, from all units in central to northwest part of study area. Data plots as great circle that defines similar F_3 fold axis as in B. Data also defines two clusters, reflecting subvertical and southeast-dipping orientation of D_3 fold limbs (as seen in sketch A), that can be used to calculate the subhorizontal average axial plane (AP_3) of D_3 folds. (D) Poles to S_{2k} cleavage from units in central to northwest part of study area, and poles to S_2 cleavage from units in southeast part of study area. S_{2k} poles define great circle with similar F_3 fold axis as in B and C. S_2 poles define a cluster, indicating that D_3 folding is largely absent in the southeast part of the range, consistent with field observations.

post-date both D_1 and D_2 deformation. D_4 structures, however, are not deformed by F_3 folds (see Section 6), and the folds therefore predate D_4 deformation.

6. D_4 deformation, Cretaceous intrusion and contact metamorphism

The final phase of Mesozoic deformation in the southern SRR occurred during intrusion of mid-Cretaceous stocks and the thermal metamorphism that accompanied intrusion. Structures produced during this deformational event are called D_4 structures, and the syntectonic thermal metamorphism is referred to as M_4. D_4 structures are recognized on the basis of syntectonic textural relations with M_4 minerals and/or occurrence only in the thermal aureoles of the Cretaceous intrusion.

The most pronounced effects of M_4 metamorphism are found in the thermal aureole of the Andorno stock (Fig. 11a), while smaller intrusions have smaller aureoles in which metamorphic recrystallization is less advanced. In the inter-aureole areas, M_4 metamorphic recrystallization is generally absent or minor, except in localized 'hornfels zones' (Fig. 11a). Structures related to D_4 deformation are found everywhere, but are most pronounced and pervasive in the thermal aureole of the Andorno stock. In the first

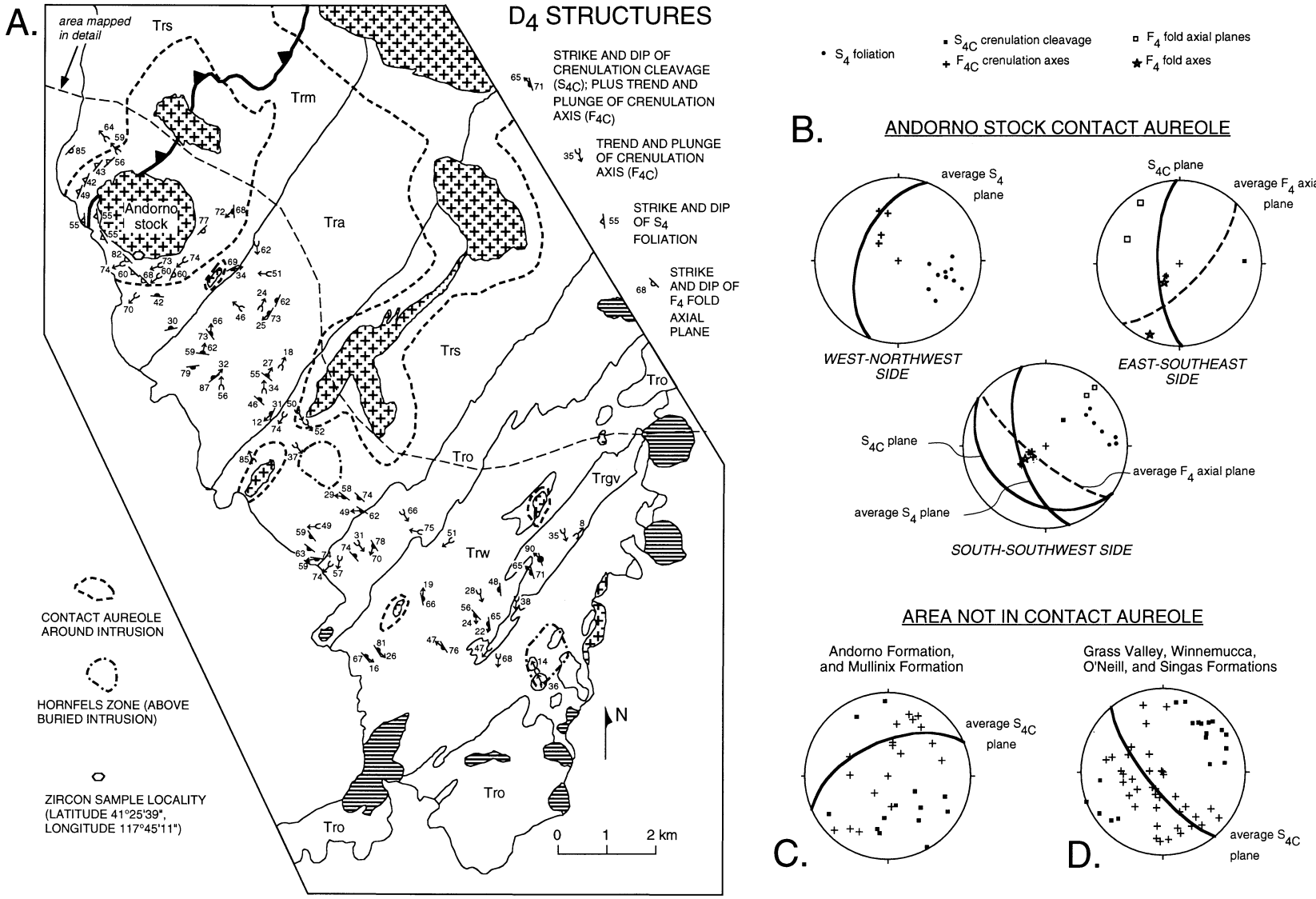

Fig. 11. (A) Map of southern Santa Rosa Range, showing location and orientation of D_4 structures, thermal metamorphic aureoles around intrusions, hornfels zones (defined in text), and location of zircon sample from Andorno stock. Aureole and hornfels zone contacts from area of detailed mapping based on our work. Aureole contacts from rest of area from Compton (1960). Triassic units not patterned to make structural symbols more evident; otherwise, patterns and unit symbols same as in Fig. 3. (B–D) Lower-hemisphere equal-area projections of orientation data for D_4 structures, emphasizing how structures and orientations vary with area. Symbols defined at top of diagram. (B) Data from metamorphic aureole of Andorno stock, divided into location within aureole relative to intrusion margins. (C) Data from central part of study area, southeast of Andorno stock aureole. (D) Data from southeastern part of study area, far from Andorno stock aureole.

section below, we present geochronologic data demonstrating that the Andorno stock was emplaced at 102 Ma. We then describe and discuss M_4 metamorphism and D_4 structures.

6.1. Age of stocks and dikes

A sample of the Andorno stock was collected for U–Pb zircon geochronologic analysis at the location shown in Fig. 11a. The sample is typical of the stock. It is a medium to coarse grained, biotite granodiorite, with anhedral to subhedral granular texture. The igneous mineralogy is 50% plagioclase, 20–25% quartz, 15–20% potassium feldspar, and 7–10% biotite. There is no magmatic fabric or evidence of solid state deformation within the sample, although biotite and plagioclase are locally partly replaced by minor amounts of chlorite, epidote and/or muscovite.

A single spot on eight separate zircon grains was analyzed using the SHRIMP-RG located at Stanford University (Table 1). All $^{206}Pb/^{238}U$ dates are indistinguishable within analytical error and we interpret the age of the Andorno stock as 102.4 ± 1.0 Ma, which is the weighted mean and 2-sigma error of the $^{206}Pb/^{238}U$ dates.

6.2. M_4 metamorphism

M_4 metamorphism, defined as metamorphism related to Cretaceous intrusions, is easily recognized in the SRR because it is most pronounced in definable aureoles around the intrusions (Fig. 11a), because it produced mineral assemblages reflecting higher temperature conditions than were associated with regional M_1 metamorphism, and because the M_4 minerals cross-cut the S_1 foliation (Fig. 12; Compton, 1960; Rogers, 1999). Depending on area, the M_4 metamorphic assemblage includes some combination of biotite ± muscovite ± andalusite ± cordierite ± staurolite, with staurolite occurring only near the margins of the largest intrusions (e.g. the Santa Rosa pluton: Fig. 3; Compton, 1960; Rogers, 1999). In our study area in the southern SRR, the M_4 assemblage consists only of biotite ± muscovite ± andalusite ± cordierite (Rogers, 1999).

Outer boundaries of thermal aureoles around intrusions in the southern SRR are shown in Fig. 11a. These boundaries were mapped by us and differ slightly from those mapped by Compton (1960). In all cases, the outer boundary was defined by the first appearance of M_4 metamorphic minerals that are visible at the hand sample scale and/or by the first appearance of pervasive hornfels textures in metapelites. The aureole around the Andorno stock extends from about 600 to 1100 m from the intrusion margin (Fig. 11a). Smaller intrusions in the southern SRR have smaller aureoles, extending from about 50 to 400 m from intrusion margins (Fig. 11a). Within the inter-aureole areas, there is generally little manifestation of M_4 metamorphism except for locally-developed spotted slates and phyllites. In addition, we were able to map some discrete zones in the inter-aureole areas in which hornfels textures are pervasive in metapelites and macroscopic M_4 minerals are visible. We call these areas hornfels zones (Fig. 11a) and interpret them to reflect contact metamorphism by near-surface Cretaceous intrusions that are not exposed.

Within the thermal aureole of the Andorno stock, the M_4 mineral assemblage in pelitic rocks includes biotite plus some combination of andalusite, cordierite, and minor muscovite (Fig. 12e–g). Andalusite forms porphyroblasts that are up to 3 cm long. Cordierite forms smaller porphyroblasts (1–2 mm diameter) that are much less common than andalusite. M_4 biotite is much more common than M_4 muscovite, the latter of which is easily distinguished from M_1 muscovite because it is larger (up to 2 mm) and because it cuts across the S_1 cleavage.

In the thermal aureoles around smaller intrusions and in the hornfels zones, a similar M_4 metamorphic assemblage is present, but andalusite is less common and cordierite is less well developed, occurring mostly as spots rather than fully formed crystals. The spots, which are also found locally in inter-aureole areas, are semi-circular to oval, vary in size from 0.3 to 2 mm, and contain higher concentrations of chlorite and lower concentrations of quartz than the remainder of the rock, which creates a dark area that defines the feature (Fig. 12b and c). In thin section, they can be traced from the initial stages of development as vague spots, to the formation of fine-grained polycrystalline

Table 1
Andorno stock zircon SHRIMP-RG isotopic data

Grain spot	Concentration (ppm)		Atomic ratios		Corrected dates (Ma)
	U	Pb[a]	$^{238}U/^{206}Pb$	$^{207}Pb/^{206}Pb$	$^{206}Pb/^{238}U$
Kas-1.1	711	11	62.5 (9)	0.05364 (116)	101.7 ± 1.5
Kas-2.1	766	12	62.5 (7)	0.05404 (144)	101.5 ± 1.1
Kas-3.1	587	9	61.6 (8)	0.05367 (130)	103.0 ± 1.3
Kas-4.1	504	8	61.3 (8)	0.05807 (134)	103.0 ± 1.4
Kas-5.1	491	8	62.2 (9)	0.05840 (156)	101.6 ± 1.4
Kas-6.1	656	10	61.5 (1.1)	0.05343 (225)	103.2 ± 1.9
Kas-7.1	503	8	60.8 (9)	0.05755 (191)	103.9 ± 1.5
Kas-8.1	633	10	61.8 (1.1)	0.05614 (204)	102.4 ± 1.9

[a] Denotes radiogenic Pb.

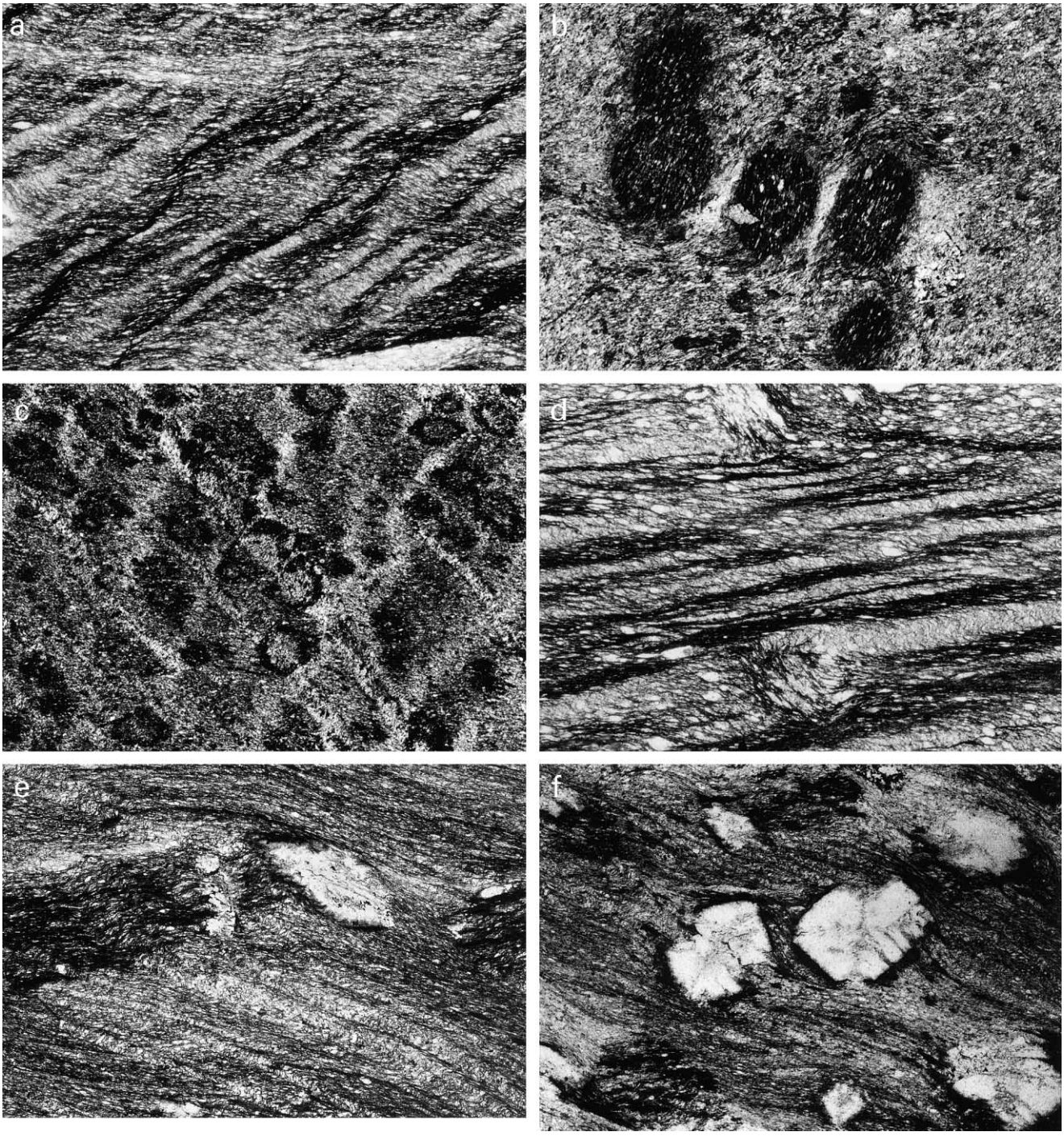

cordierite, and eventually into single cordierite crystals (Rogers, 1999). Similar spots, grading into fully formed cordierite, are found in the thermal aureole of the Andorno stock (Fig. 12e and f). We thus conclude that spots in slates and phyllites reflect incipient growth of cordierite during metamorphic recrystallization related to Cretaceous intrusive activity. The interpretation is that spot growth is the result of heating from intrusions, but that the intrusions were sufficiently small or distant that not enough heat was supplied in most cases to fully carry out the metamorphic reaction and form well-developed cordierite.

Rock texture associated with M_4 metamorphism varies spatially in the southern SRR. In the inter-aureole areas, the S_1 cleavage is still clearly defined in slates and phyllites and the only manifestation of M_4 metamorphism is the locally-developed spots. In the hornfels zones and the aureoles of the smaller intrusions, the S_1 cleavage is partly to largely obscured by growth of randomly-oriented M_4 minerals, and metapelitic rocks have an obvious hornfels texture. On the east side of the Andorno stock, slates, phyllites and quartzites have been transformed into dense, sugary hornfels due to extensive growth of randomly-oriented M_4

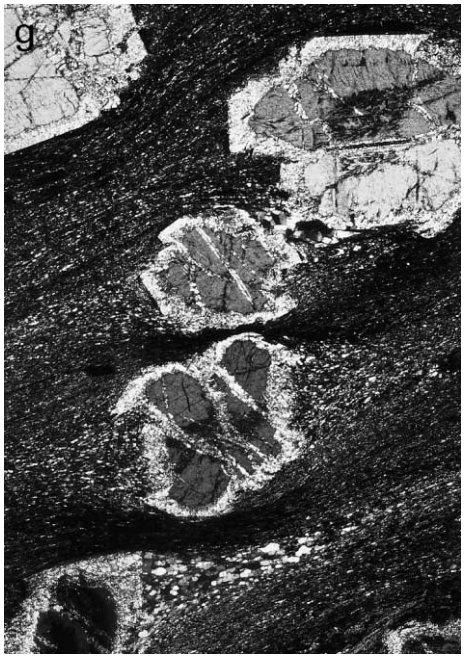

Fig. 12. (*continued*)

metamorphic minerals. Elsewhere around the Andorno stock, however, the M_4 minerals grew concurrently with D_4 deformation, and they define a variably-developed S_4 foliation, as described in Section 6.3.

6.3. D_4 deformation

D_4 structures in the southern SRR are recognized based on their syntectonic textural relationship with M_4 minerals, on their localized occurrence only in the thermal aureoles of Cretaceous intrusions, and/or on cross-cutting relations indicating that the structures post-date D_1, D_2 and D_3 deformation. Syntectonic textural relations are defined based on standard practice, using microtextural data on porphyroblasts and foliations (Spry, 1969; Barker, 1990; Yardley, 1990). The D_4 structures are described first, followed by a discussion of evidence that they formed during M_4 thermal metamorphism.

The most common D_4 structures are crenulations of the S_1 cleavage, and an associated crenulation cleavage (S_{4C}) in slates and phyllites (Figs. 11a and 12a–e). These structures are found locally throughout the inter-aureole areas, and are also present in the hornfels zones, the thermal aureoles of smaller intrusions, and locally within the thermal aureole of the Andorno stock. In inter-aureole areas, S_{4C} is a spaced cleavage that is developed on the limbs of the crenulations, and is defined by decreased concentration of quartz and increased concentration of muscovite and opaques, relative to the microlithon areas between cleavage planes (Fig. 12a), indicating formation by pressure solution processes. This S_{4C} cleavage cuts the S_1 cleavage at a moderate to steep angle everywhere, as it does with the S_{2k} kink band fabric and S_2 spaced cleavage (Figs. 9c–e and 12a–e).

Crenulations of the S_1 foliation are also found in metapelitic rocks in the thermal aureole of the Andorno stock (Fig. 11a). These structures are most evident in the south part of the aureole. Here, they are similar to D_4 crenulations elsewhere in the study area, except they have a somewhat better developed S_{4C} cleavage which is defined in part by aligned M_4 biotite (Fig. 12d and e). In the southwest part of the aureole, the crenulation fabric grades locally into a continuous S_4 foliation that parallels the S_{4C} crenulation cleavage but is defined by the preferred alignment of closely-spaced M_4 mica with no crenulated microlithon domains visible (Fig. 12e and f). Moving into the west and northwest parts of the aureole, the S_4 foliation becomes increasingly prevalent and pervasive (Fig. 11a). Here, it imparts a phyllitic texture to all metapelitic rocks, and it generally completely overprints the S_1 cleavage (Fig. 12g). Additional D_4 structures, found only in the Andorno

Fig. 12. Photomicrographs showing D_4 structures and M_4 metamorphism in the southern SRR. (A,B) O'Neill Formation slates from inter-aureole area; both plain light, long dimension 3.2 mm. (A) D_4 crenulations and S_{4C} crenulation cleavage (oriented lower left to upper right) cut across S_1 slaty cleavage (horizontal). (B) Spots (incipient M_4 cordierite) and D_4 crenulations cut across S_1 cleavage. Spots contain internal S_1 cleavage oriented ~190 to 10°. S_1 cleavage outside of spots oriented generally ~240 to 60°, but is reoriented near spots by weak crenulations whose axial traces trend ~280 to 100°. Light areas at ends of spots are pressure shadows containing abundant quartz. (C) Singas Formation metapelite in aureole of small Cretaceous stock in central part of study area near range front (see Fig. 4). S_1 cleavage (weakly visible) approximately horizontal. S_{2k} kink bands (oriented lower left to upper right) form irregular light colored bands. S_{4C} spaced crenulation cleavage (oriented lower right to upper left) cuts S_1 and S_{2k}. Circular spots with dark rims are incipient M_4 cordierite that cut across S_{4C} and all older fabrics. Cross-nicols; long dimension 3.2 mm. (D–G) Samples from Mullinix and Singas Formation metapelites in thermal aureole of Andorno stock. (D) From south side of aureole. Spaced S_{4C} crenulation cleavage (oriented lower left to upper right and defined by opaque material and minor M_4 biotite) cuts S_1 cleavage (oriented lower right to upper left, and visible only in microlithon domains). Plain light; long dimension 3.2 mm. (E) From southwest side of aureole. Spots (incipient M_4 cordierite) are large dark patches on left and right; M_4 andalusite porphyroblast (white) is in center. D_4 crenulations and S_{4C} crenulation cleavage (visible below spot and andalusite) grade into closely spaced S_4 foliation (above andalusite), and all trend from upper left to lower right. S_{4C} and S_4 defined by aligned M_4 biotite and minor muscovite. S_1 cleavage (oriented lower left to upper right) visible in crenulation cleavage microlithons, and in spots where it has a weakly crenulated geometry. Plain light, long dimension 5.5 mm. (F) Same sample as E. S_{4C} crenulation cleavage grades locally into continuous S_4 foliation; both trend from upper left to lower right and are defined by aligned M_4 biotite and minor muscovite. S_1 cleavage (oriented lower left to upper right) visible in S_{4C} microlithon domains. Note that S_{4C} and S_4 trend into ends of M_4 andalusite porphyroblasts (white) but also bend weakly around them. Dark patch in lower left is incipient M_4 cordierite spot. Plain light, long dimension 6.5 mm. (G) From west side of aureole. Continuous S_4 foliation, defined by aligned M_4 biotite, trends from lower left to upper right. S_1 no longer visible. Note that long axes of M_4 andalusite porphyroblasts (white) parallel S_4, that S_4 bends weakly around porphyroblasts but also trends into their ends, and that pressure shadows on ends of andalusites are composed of fine grained quartz and aligned M_4 mica. Cross-nicols, long dimension 5.0 mm.

aureole, include larger-scale F_4 folds in quartzite beds (Fig. 11a). These folds are open to close in limb appression, and parallel in shape, with decimeter-scale wavelengths. They do not have an axial planar foliation that can be linked to the M_4 metamorphic assemblage; however, there are several reasons to conclude that they formed during M_4 metamorphism and synchronous D_4 deformation, as described below.

A variety of lines of evidence indicates that all D_4 structures described above formed after D_{1-3} deformation and during M_4 metamorphism.

1. Cross-cutting relations clearly indicate that the crenulation structures in the southern SRR post-date D_1, D_2 and D_3 deformation. This conclusion is based on the following. The crenulations deform the S_1 foliation, and the associated S_{4C} cleavage cuts across the S_1 foliation, and both features therefore post-date D_1 deformation (Fig. 12a–e). The S_{4C} cleavage cross-cuts the S_2 cleavage and the S_{2k} kink-band fabric, wherever the two are found together (Figs. 9c–e and 12c), and crenulations therefore post-date D_2 deformation. The crenulations post-date D_3 folding because they have not been reoriented or folded about the NE-trending subhorizontal fold axes associated with D_3 folds (see Section 6.4).
2. The crenulation structures in the southern SRR can be directly assigned to a D_4 deformational phase based on microtextural relations between crenulations and M_4 spots (incipient cordierite). Several different types of microtextural relations are seen. In some rocks, the spots contain a relict internal S_1 cleavage that is planar and of similar orientation in all the spots (Fig. 12b). In these rocks, the crenulations bend weakly around the spots, and there are pressure shadows at the ends of the spots in which no foliation is visible (Fig. 12b). These spots thus grew prior to formation of the crenulations. In some rocks, the relict internal S_1 cleavage in spots is weakly crenulated, and these internal crenulations track into better developed crenulations, associated with a crenulation cleavage, in the areas outside the spots (Fig. 12e). These spots thus grew during development of the crenulation structures. Finally, in some rocks, the spots grow across the crenulations and crenulation cleavage (Fig. 12c). These spots thus grew after development of the crenulation fabric. Collectively, this combination of relations can only be reconciled if crenulation development and M_4 thermal metamorphism were broadly synchronous.
3. In the aureole of the Andorno stock, crenulations and the continuous phyllitic foliation can be directly assigned to a D_4 deformational phase based on their microtextural relations with M_4 andalusite porphyroblasts. Several microtextural relations are key to this conclusion. First, the crenulations are cut by andalusite porphyroblasts but also bend weakly around them (Fig. 12f). Second, the crenulation cleavage grades progressively into the similarly-oriented continuous phyllitic foliation, and both are defined at least in part by M_4 biotite (Fig. 12d–g). Third, the continuous phyllitic foliation bends around the andalusite porphyroblasts but also tracks into their ends where pressure shadows composed of quartz and minor aligned M_4 mica are evident (Fig. 12f and g). Finally, long axes of andalusite porphyroblasts are always aligned within the plane of the continuous phyllitic foliation (Fig. 12g). Collectively, these relations indicate an overlap in timing between crenulation development, continuous phyllitic foliation development, and growth of M_4 andalusite in the metamorphic aureole of the Andorno stock.
4. D_4 folds in the aureole of the Andorno stock, defined on the basis of their shape, size and orientation, are found only within the confines of the aureole and have a similar geometry to D_4 structures in nearby parts of the aureole (Fig. 11). In addition, these folds fold the S_1 cleavage and therefore must post-date D_1 deformation; they are unlikely to be related to D_2 deformation because D_2 structures elsewhere in the northwest part of the study area consist only of heterogeneously-distributed kink bands that reflect very minor shortening; and they are also unlikely to be related to D_3 deformation because they have steeply dipping axial planes (Fig. 11), which is inconsistent with the geometry of F_3 folds. Collectively, these relations are most consistent with a conclusion that these folds formed during D_4 deformation in the thermal aureole of the Andorno stock.

6.4. Orientation of D_4 structures

The orientation of D_4 structures varies systematically across the study area, as shown in the map and stereonets of Fig. 11. The variations indicate that multiple processes acted to influence D_4 structures, as explained below.

Structural data shown in Fig. 11a and b indicate that D_4 structures within the Andorno stock aureole have orientations that vary consistently with the orientation of the adjacent intrusion margin. Along the NE-striking eastern margin of the stock, F_4 fold axial planes strike NE and dip steeply to the SE; along the WNW-striking southern margin of the stock, F_4 fold axial planes strike NW and dip steeply to the SW; and along the N-striking western margin of the stock, the S_4 foliation strikes to the N and dips steeply to the W (Fig. 11a and b). These relations indicate that the axis of principal shortening strain during D_4 deformation in the Andorno aureole was everywhere broadly perpendicular to the margins of the intrusion. The variation in orientation of D_4 structures around the Andorno stock provides evidence that development of these structures was influenced by stresses related to intrusion that were directed radially outward from the intrusion margin.

Outside of the Andorno stock aureole, within the inter-aureole areas, the orientation of D_4 structures also varies

spatially but less profoundly than within the aureole (Fig. 11a, c and d). In the central and southeastern part of the study area, the crenulation cleavage (S_{4C}) strikes NW and dips steeply to the SW, and crenulation axes plunge generally to the west and south within the cleavage plane (Fig. 11a and d). Moving to the northwest, closer to the contact aureole of the Andorno stock, however, the orientation of the crenulation fabric changes. Here, the crenulation cleavage generally strikes NE and dips steeply to the NW, and crenulation axes plunge more to the west and north within the cleavage plane (Fig. 11a and c). This orientation is more like the orientation of D_4 structures on the east side of the Andorno stock contact aureole (Fig. 11a and b).

6.5. Summary and interpretation of D_4

Intrusion of mid-Cretaceous (102 Ma) granitoid stocks and dikes resulted in widespread thermal metamorphism (M_4) within the Triassic strata of the southern SRR. The effects of this metamorphic overprint are most pronounced near the larger intrusions, where metamorphic aureoles are well-developed, but can also be seen to some degree within inter-aureole areas.

Intrusion was accompanied by a D_4 phase of deformation based on syntectonic textural relations with M_4 mineral assemblages, restriction of these structures to intrusion aureoles, and/or cross-cutting relations with older structures. These D_4 structures consist mostly of a heterogeneously-developed, spaced crenulation fabric within slates and phyllites, except in the aureole of the Andorno stock where the D_4 crenulation is upgraded to a continuous phyllitic foliation, and larger-scale folding is locally evident.

The orientations of D_4 structures vary across the study area in a manner indicating that they were influenced by stresses associated with emplacement of the mid-Cretaceous stocks, in particular the Andorno stock. The effects of D_4 deformation are seen too far from intrusions and are too widespread across the study area, however, to be reasonably attributed solely to forceful pluton emplacement. Furthermore, D_4 structures farthest from the Andorno stock have a consistent NW strike and sub-vertical dip. These relations argue that D_4 deformation in the SRR reflects regional shortening in a NE–SW direction, with modification to this regional strain-field occurring only near the larger syntectonic intrusions.

The amount of regional strain implied by inter-aureole D_4 structures in the southern SRR is minor. Estimates of the amount of shortening represented by crenulations such as in Fig. 12a indicate ~10% shortening. This is a maximum, however, because the crenulation fabric is only locally developed within the inter-aureole areas. Substantially greater strain is represented by D_4 structures around the Andorno stock.

7. Correlative deformation in the northern LFTB

In order to place the structural data discussed above into a more regional perspective, it is important to compare deformational phases identified in the southern SRR with deformational phases identified by other workers elsewhere in the LFTB. This comparison allows correlations to be made between structures in different areas, which is critical to a regional analysis of the structural evolution of the LFTB. For the purposes of comparison, we focus only on nearby areas (Fig. 2), including the Eugene Mountains (Thole and Prihar, 1998), the northern East Range (Elison and Speed, 1989), and the Jungo area and Blue Mountain (Wyld, 1998; Folsom, 2000).

7.1. D_1 deformation

The characteristic features of D_1 deformation in the southern SRR are: tight to isoclinal folds of bedding, with NE–SW trending and shallowly-plunging fold axes, and a general asymmetry indicating top-to-the-SE vergence; a pervasive axial-planar cleavage that strikes NE and dips NW; and top-to-the-SE reverse faulting. This phase of deformation produced the main structural grain within the Triassic basinal terrane and reflects shortening of at least 55–70%.

Obviously identical structures are easily recognized elsewhere in the northern LFTB. Specifically, first-generation structures in the Eugene Mountains, northern East Range, Blue Mountain, and Jungo consist of tight to isoclinal folds of bedding, a pervasive axial-planar cleavage, and thrust faults (Elison and Speed, 1989; Oldow et al., 1990; Thole and Prihar, 1998; Wyld, 1998, Folsom, 2000). In all areas, these first-generation structures form the dominant structural grain within the Triassic strata, and reflect NW–SE shortening and tectonic transport to the SE, as in the SRR. The amount of shortening during first-phase deformation has been calculated in the East Range to be 50–70% (Elison and Speed, 1989), similar to that in the SRR.

Collectively, the similarities listed above provide a compelling argument that all first-generation structures in the northern basinal terrane reflect the same phase of deformation, and that this phase of deformation is pervasive and major within the northern LFTB. Because there is no structural evidence for any deformation preceding D_1 in the southern SRR or any other areas noted above in the northern LFTB, we therefore conclude that D_1 constitutes the first phase of deformation in the northern LFTB. As noted earlier, age data from the SRR and from other areas of the northern basinal terrane argue that D_1 deformation occurred in the late Early and/or early Middle Jurassic (Quinn, 1996; Wyld et al., 1999; Folsom, 2000; Wyld and Wright, 2000).

7.2. D_2 deformation

Characteristic features of D_2 deformation in the southern SRR are as follows. First, D_2 structures are only locally-developed, and reflect increasing strain toward the

southeast, potentially toward a reverse fault buried beneath Quaternary alluvium east of the range. Second, D_2 structures include open to close, parallel folds, and a locally-developed spaced cleavage. The folds have subhorizontal, NE–SW trending axes with NW-dipping axial planes that parallel the cleavage.

Similar second-generation structures are found elsewhere in the northern basinal terrane, but only in areas near the frontal Fencemaker thrust of the LFTB. Thus, similar second-generation structures are found in the northern East Range, but are absent in the Eugene Mountains and the Jungo–Blue Mountain area (Fig. 2; Elison and Speed, 1989; Oldow et al., 1990; Thole and Prihar, 1998; Wyld, 1998; Folsom, 2000). In the East Range, second-generation structures include: gentle to close folds; a locally-developed, spaced, axial-planar cleavage; and some NW-dipping thrust and reverse faults. These structures reflect NW–SE shortening, as in the southern SRR. Significantly, D_2 strain in the East Range increases toward the faults (Elison and Speed, 1989). These relations are consistent with, and supportive of, our conclusion that the D_2 strain gradient in the southern SRR reflects increasing proximity toward a buried D_2 fault east of the range. Elison and Speed (1989) also point out that D_2 strain in the East Range is greatest near the Fencemaker thrust, and that it is only near this fault that any significant development of an S_2 cleavage occurs. In view of the fact that the Fencemaker thrust is located just to the east of the southern SRR (Fig. 2), these relations suggest that D_2 deformation in the SRR may also be related to displacement along the Fencemaker thrust.

Restriction of D_2 deformation in the northern LFTB to the eastern margin of the province, near the Fencemaker thrust, suggests that this phase of deformation may be related to final emplacement of the basinal terrane over coeval shelf strata along the thrust. Elison and Speed (1989) drew a similar conclusion based on structural relations in the northern East Range.

As noted earlier, D_2 deformation in the SRR can only be constrained to have occurred sometime in the Middle Jurassic to Early Cretaceous interval. Correlation of D_2 structures in the SRR with those in the northern East Range provides further insight into timing relations. In the latter area, D_2 structures are cross-cut by a fault that is in turn cut by a pluton dated at 153 (K/Ar; Elison, 1995). Considering this data plus the Early and/or Middle Jurassic age of D_1 deformation, we conclude that D_2 deformation in the northern LFTB likely took place sometime in the Middle to early Late Jurassic interval.

7.3. D_3 deformation

D_3 deformation in the southern SRR produced large, gentle folds of earlier structures that reflect a minor amount of shortening (<5%). These structures reflect broadly pure shear deformation with subvertical shortening and subhorizontal extension, and are prevalent only in the northwest part of the study area. They formed after D_2 deformation (after Middle or Late Jurassic) but prior to D_4 deformation in the mid-Cretaceous (102 Ma).

No similar structures have been described from any of the other areas studied in detail within the northern LFTB (i.e. the northern East Range, southern Humboldt Range, Eugene Mountains, Blue Mountain, and Jungo area: Elison and Speed, 1989; Oldow et al., 1990; Thole and Prihar, 1998; Folsom, 2000; Wyld, 1998, 2000). This suggests that D_3 deformation in the southern SRR could reflect some process unique to this area. One possibility is that D_3 deformation in the SRR could reflect strain associated with emplacement of Cretaceous magma bodies. There are two reasons for suggesting this conclusion. (1) D_3 deformation in the southern SRR is restricted to the central and northwest parts of the area where Cretaceous intrusions are most abundant (Figs. 3 and 4). This suggests that the presence of D_3 deformation is related in some way to intrusion. (2) In the SRR, where D_3 deformation is recognized, Cretaceous intrusions are abundant and large (Figs. 2 and 3), whereas in other areas of the northern LFTB where no D_3 deformation is recognized (northern East Range, southern Humboldt Range, Eugene Mountains, Blue Mountain, and Jungo area), Cretaceous intrusions are either absent, or small and uncommon (Elison and Speed, 1989; Oldow et al., 1990; Thole and Prihar, 1998; Rogers, 1999; Wyld, unpublished data). This also suggests that the presence of D_3 deformation is related in some way to intrusion. If this interpretation is correct, the kinematic model would be that the early stages of voluminous magma emplacement into the SRR resulted in subvertically-oriented compressive stresses that produced broad folds with subhorizontal axial planes within Triassic strata overlying the rising magma bodies.

In the absence of any additional information (for example from other areas that might be found to contain equivalent structures), it is difficult to further evaluate the possible origin or cause of D_3 deformation in the SRR. Fortunately, a lack of in-depth understanding of this phase of deformation is of little regional significance, because the amount of shortening associated with it is very small and because it has had a very limited area of impact in the northern LFTB.

7.4. D_4 deformation

The most distinctive features of D_4 deformation in the southern SRR are: that it occurred during intrusion of mid-Cretaceous (102 Ma) stocks and the thermal metamorphism associated with these intrusions; that it reflects regional shortening in a NE–SW direction, upon which is superimposed local strain associated with emplacement of the Andorno stock; and that the regional D_4 shortening is minor and is primarily manifested by heterogeneously-distributed, spaced crenulations and crenulation cleavage in slates and phyllites.

Similar late-phase structures are found elsewhere throughout the northern basinal terrane. Thus, late-phase

structures in the northern East Range, Eugene Mountains, Blue Mountain, and Jungo include crenulations with a spaced crenulation cleavage, and/or gentle to open larger folds with a locally-developed spaced cleavage (Elison and Speed, 1989; Thole and Prihar, 1998; Wyld, 1998; Folsom, 2000; Wyld and Wright, 2000). In all cases, these late-phase structures are only locally-developed, reflect minor shortening, and have orientations indicative of NE–SW shortening, as in the SRR. In addition, Thole and Prihar (1998) indicate that late phase structures in the Eugene Mountains increase in strain toward the margins of Cretaceous intrusions, and suggest that these structures are related to forceful intrusion, similar to our interpretation of D_4 structures in the aureole of the Andorno stock in the SRR.

Collectively, the similarities listed above between D_4 structures in the southern SRR and late-phase structures elsewhere in the northern basinal terrane lead to the conclusion that these structures all reflect the same deformational event. Structures developed during this event accommodated minor shortening in a generally NE–SW direction, but were also influenced by strain associated with emplacement of syntectonic intrusions. The timing of this event is well-constrained by the 102 Ma age of syntectonic intrusions in the SRR. Broadly similar age relations are defined in the Eugene Mountains, where late-stage shortening structures are associated with Cretaceous granitoid stocks dated at 76–89 Ma by the K/Ar method (Thole and Prihar, 1998).

8. Interpretation and structural model

Our data from the SRR, coupled with relations in nearby areas, can be combined into a new detailed interpretation of the structural evolution of the northern LFTB. Our study and analysis shows that two broad periods of deformation affected rocks in this region. The first occurred in the Jurassic and is represented by D_1 and D_2 structures which both reflect generally NW–SE shortening. The second occurred over 50 m.y. later in the mid-Cretaceous and is represented by D_4, and possibly D_3, structures, which both reflect very different shortening directions from D_1 and D_2. The relations we have discussed lead to the further conclusion that only the earlier D_1 and D_2 phases of deformation can be tied to the development of the northern LFTB as an evolving fold-thrust belt structural province. D_3 and D_4 deformation, in contrast, reflect unrelated younger processes. Below, we elaborate on these points, and use the new database to develop a new regional model of the structural evolution of this part of the Cordillera.

8.1. D_1 and D_2: Jurassic back-arc basin closure and development of the LFTB

As noted in Section 1, early Mesozoic strata of the basinal terrane were deposited within a back-arc basin that was deep marine in the Late Triassic but shoaled to shallower water depths in the Early Jurassic. Development of the LFTB evidently resulted in structural closure of this back-arc basin, as no younger marine strata are recognized in this part of Nevada. The deformational history of the LFTB is therefore an example of processes that operate during structural closure of a back-arc basin. The tectonic driving force for back-arc compression in this area is not presently known with certainty; however, arc assemblages west of the LFTB also suffered widespread deformation in the Jurassic, suggesting that shortening within the arc and back-arc regions was related and a result of either strongly coupled plate convergence or collision at the plate margin (e.g. Burchfiel et al., 1992).

Our data from the SRR indicate that the first phase of deformation to affect the northern basinal terrane (D_1) involved substantial NW–SE shortening by folding, cleavage development under low-grade metamorphic conditions, and reverse faulting. Regional relations indicate that this D_1 phase of deformation is present throughout the northern basinal terrane, and everywhere represented by strikingly similar structures, from the Jungo area near the contact of basinal rocks with the Black Rock arc terrane, through more centrally located areas like the SRR, to the East Range near the Fencemaker thrust contact between basinal terrane rocks and the shelf province (Fig. 2; cf. Oldow, 1984). In all areas, D_1 deformation produced the dominant structural grain within the basinal rocks and, where measured, was associated with substantial shortening, on the order of $\geqq 50$–70%.

Collectively, these data argue that structural closure of the early Mesozoic back-arc basin took place primarily during the D_1 phase of deformation. The process of back-arc basin collapse occurred via development of a top-to-the-SE fold-thrust belt, but it is important to emphasize that this fold-thrust belt is characterized primarily by ductile structures (pervasive cleavage and tight to isoclinal folds). It therefore differs in style from that of many typical foreland fold-thrust belts where shortening is accommodated primarily by brittle thrusts and more open folding. This difference presumably reflects the subgreenschist to low greenschist grade metamorphic conditions that prevailed during D_1 deformation, which promoted ductile behavior in the shales that made up the majority of the deforming strata. Elevated temperature conditions are believed to reflect tectonic burial of the basinal terrane strata during D_1 deformation via internal thrust imbrication within the basin as well as thrusting of the Black Rock arc terrane over the western basinal terrane (Wyld, 1998, 2000; Rogers, 1999).

D_1 deformation in the northern basinal terrane was followed in some places by a D_2 phase of deformation. Our data from the SRR indicate that this D_2 deformation reflects a similar strain regime to D_1 but less overall shortening and less ductile conditions. Our data also indicate that D_2 strain dies out from east to west in the SRR. This is consistent with regional evidence that D_2 deformation is only present in the eastern part of the basinal

terrane near the frontal Fencemaker thrust of the LFTB. Collectively, these relations suggest that D_2 deformation within the northern LFTB was associated with final emplacement of the basinal terrane over coeval shelf deposits along the Fencemaker thrust.

Insofar as D_2 deformation is older than mid-Late Jurassic, the entire development of the LFTB within the northern basinal terrane took place in the Jurassic, between the late Early Jurassic and the late Late Jurassic (~153 Ma). Furthermore, our data indicate that the northern LFTB developed primarily during a single phase of deformation (D_1) in the Early–Middle Jurassic, and that polyphase thrust belt deformation ($D_1 + D_2$) that may have extended into the Late Jurassic is restricted to the eastern part of the belt.

8.2. D_3 and D_4: mid-Cretaceous intra-arc shortening

The final phase of Mesozoic deformation in the SRR, D_4, occurred during intrusion of mid-Cretaceous (102 Ma) granodiorite to tonalite stocks, dikes and plutons. D_3 deformation is also interpreted to be related to intrusion, although timing constraints for this very minor and localized phase of deformation are not as well defined as they are for the more widespread D_4 structures. The intrusions form part of a suite of mid-Cretaceous, arc-related granitoid plutons that are locally common within the basinal terrane (Fig. 2) and merge westward into the Cretaceous batholithic belt of the western US Cordillera (Fig. 1). The presence of these intrusions within the basinal terrane indicates that, by mid-Cretaceous time, the basinal terrane was no longer in a back-arc position, but was instead actually more within the arc, albeit on its margins; quantitatively, the basinal terrane is within the area of >30% density of Cretaceous plutons defined by Barton et al. (1988). Deformation within the basinal terrane during this time-frame therefore represents more intra-arc than back-arc deformation. Consistent with this change in tectonic environment, much of the younger deformation in the SRR is closely associated with emplacement of the Cretaceous intrusions.

D_3 deformation in the SRR accommodated minor sub-vertical shortening and most likely reflects stresses associated with upward movement of voluminous Cretaceous magmas. No similar deformation is recognized elsewhere in the northern basinal terrane, but this is probably because no other areas that are as pervasively intruded by Cretaceous plutons as the SRR have been studied in any detail.

D_4 deformation in the SRR reflects regional shortening coupled with localized strain associated with final emplacement of the mid-Cretaceous intrusions. Far from the intrusions, D_4 structures include a crenulation fabric in slates and phyllites that reflects minor overall NE–SW shortening. Closer to large intrusions, M_4 thermal metamorphism becomes pronounced, and D_4 strain increases. Here, D_4 structures include larger folds and a continuous foliation that primarily indicate shortening perpendicular to intrusion margins. Thus, D_4 deformation in the SRR is a weak regional deformation that was overwhelmed by intrusion-related strain near larger intrusions. Evidence for this weak mid-Cretaceous regional deformation is found throughout the northern basinal terrane in the form of heterogeneously-developed, relatively open folds and crenulations that reflect generally NE–SW directed shortening.

The timing of Cretaceous deformation in the SRR (102 Ma) is quite similar to the time at which major shortening began in the Sevier fold-and-thrust belt and its hinterland (Fig. 1; Armstrong, 1968; Lawton, 1985; Heller et al., 1986). The thin-skinned Sevier fold-thrust belt developed within continental rocks east of the LFTB, primarily from the late Early Cretaceous (~120–100 Ma) to the earliest Tertiary, and is one of the principle manifestations of the Sevier orogeny. Deeper-seated ductile deformation in the hinterland of the Sevier Belt, in eastern Nevada, occurred primarily from ~110–73 Ma (Miller et al., 1988; Snoke and Miller, 1988; Smith et al., 1993). We suggest that similar-age Cretaceous shortening further west within the northern basinal terrane is most likely an additional manifestation of this orogenic event. This helps to resolve a long-standing problem in the US Cordillera concerning whether the effects of the Sevier orogeny can be recognized west of the Sevier fold-thrust belt and its hinterland. Clearly, however, the amount of shortening recorded during the Sevier orogeny in the basinal terrane is much less than is recorded farther east in the Sevier fold-thrust belt and its hinterland.

Acknowledgements

This research was supported by the National Science Foundation grant EAR-9796174 and the Bernadette Allard Fund and Wheeler-Watts Fund (both from the University of Georgia). The research and paper have benefited from discussions with Heather Folsom, Robert Hawman, Steve Holland, Brian McNulty, John Oldow and Paul Schroeder. The final version of the paper was significantly improved by the helpful comments of reviewers John Oldow and Robert Wintsch. We gratefully acknowledge the generosity of Leon Fry of Nevada for his help with field logistics.

References

Armstrong, R.L., 1968. Sevier orogenic belt in Nevada and Utah. Geological Society of America Bulletin 79, 429–458.

Barker, A.J., 1990. Introduction to Metamorphic Textures and Microstructures. Chapman and Hall, New York.

Barton, M.D., Battles, D.A., Bebout, G.E., Capo, R.C., Christianson, J.N., Davis, S.R., Hanson, R.B., Michelson, C.J., Trim, H.E., 1988. Mesozoic contact metamorphism in the western United States. In: Ernst, W.G. (Ed.). Metamorphism and Crustal Evolution, Western Coterminous United States, Vol. 7. Prentice-Hall, Englewood Cliffs, NJ, pp. 111–178.

Borradaile, G.J., Bayly, M.B., Powell, C.McA. (Eds.), 1982. Atlas of Deformation and Metamorphic Rock Fabrics Springer-Verlag, New York.

Burchfiel, B.C., Cowan, D.S., Davis, G.A., 1992. Tectonic overview of the Cordilleran orogen in the western United States. In: Burchfiel, B.C., Lipman, P.W., Zoback, M.L. (Eds.). The Geology of North America, v. G-3, The Cordilleran Orogen. Conterminous US Geological Society of America, Boulder, CO, pp. 407–479.

Burke, D.B., Silberling, N.J., 1973. The Auld Lang Syne Group, of Late Triassic and Jurassic (?) Age, North-Central Nevada. Geological Survey Bulletin 1394, E1–E14.

Compton, R.R., 1960. Contact metamorphism in the Santa Rosa Range, Nevada. Geological Society of America Bulletin 71, 1383–1416.

Elison, M.W., 1995. Causes and consequences of Jurassic magmatism in the northern Great Basin: implications for tectonic development. In: Miller, D.M., Busby, C. (Eds.). Jurassic Magmatism and Tectonics of the North American Cordillera. , pp. 249–266 Geological Society of America Special Paper 299.

Elison, M.W., Speed, R.C., 1989. Structural development during flysch basin collapse: the Fencemaker allochthon, East Range, Nevada. Journal of Structural Geology 11, 523–538.

Folsom, H.K., 2000, Analysis of Mesozoic deformation in a backarc basin, northwestern Nevada. Senior Honor's thesis, University of Georgia, Athens, 92pp.

Heck, F.R., Speed, R.C., 1987. Triassic olistostrome and shelf-basin transition in the western Great Basin: Paleogeographic implications. Geological Society of America Bulletin 99, 539–551.

Heller, P.L., Bowdler, S.S., Chambers, H.P., Coogan, J.C., Hagen, E.S., Shuster, M.W., Winslow, N.S., Lawton, T.F., 1986. Time of initial thrusting in the Sevier Orogenic belt, Idaho–Wyoming and Utah. Geology 14, 388–391.

Ho, N.-C., Peacor, D.R., van der Pluijm, B.A., 1995. Reorientation mechanisms of phyllosilicates in the mudstone-to-slate transition at Lehigh Gap, Pennsylvania. Journal of Structural Geology 17, 345–356.

Knipe, R.J., 1981. The interaction of deformation and metamorphism in slates. Tectonophysics 78, 249–272.

Lawton, T.F., 1985. Style and timing of frontal structures, thrust belt, central Utah. American Association of Petroleum Geologist Bulletin 69, 1145–1159.

Lupe, R., Silberling, N.J., 1985. Genetic relationship between Lower Mesozoic continental strata of the Colorado Plateau and Marine Strata of the Western Great Basin: significance for accretionary history of Cordilleran Lithotectonic terranes. In: Howell, D.G. (Ed.). Tectonostratigraphic Terranes of the Circum-Pacific Region. Circum-Pacific Council for Energy and Mineral Resources, pp. 263–270 Earth Science Series 1.

Miller, E.L., Gans, P.B., Wright, J.E., Sutter, J.F., 1988. Metamorphic history of the east-central Basin and Range province: Tectonic setting and relationship to magmatism. In: Ernst, W.G. (Ed.). Metamorphism and crustal evolution, western coterminous United States, Vol. 7. Prentice-Hall, Englewood Cliffs, NJ, pp. 649–682.

Oldow, J.S., 1984. Evolution of a Late Mesozoic Back-Arc Fold and Thrust Belt, Northwestern Great Basin, USA. Tectonophysics 102, 245–274.

Oldow, J.S., Bartel, R.L., Gelber, A.W., 1990. Depositional setting and regional relationships of basinal assemblages: Pershing Ridge Group and Fencemaker Canyon sequence in northwestern Nevada. Geological Society of America Bulletin 102, 193–222.

Passchier, C.W., Trouw, R.A.J., 1996. Microtectonics. Springer-Verlag, Berlin.

Quinn, M.J., 1996. Pre-Tertiary stratigraphy, magmatism, and structural history of the central Jackson Mountains, Humboldt County, Nevada. Ph.D. thesis. Rice University, Houston, Texas.

Quinn, M.J., Wright, J.E., Wyld, S.J., 1997. Happy Creek igneous complex and tectonic evolution of the early Mesozoic arc in the Jackson Mountains, northwest Nevada. Geological Society of America Bulletin 109, 461–482.

Ramsay, J.G., Huber, M.I., 1987. The Techniques of Modern Structural Geology. Volume 2: Folds and Fractures. Academic Press, New York.

Rogers, J.W., 1999. Jurassic–Cretaceous deformation in the Santa Rosa Range, Nevada: implications for the development of the northern Luning–Fencemaker fold-and-thrust belt. M.S. thesis. University of Georgia, Athens.

Saleeby, J.B., Busby-Spera, C., 1992. Early Mesozoic tectonic evolution of the western US Cordillera. In: Burchfiel, B.C., Lipman, P.W., Zoback, M.L. (Eds.). The Geology of North America, v. G-3, The Cordilleran Orogen. Conterminous US Geological Society of America, Boulder, CO, pp. 107–168.

Smith, J.G., McKee, E.H., Tatlock, D.B., Marvin, R.F., 1971. Mesozoic granitic rocks in northwest Nevada: a link between the Sierra Nevada and Idaho batholiths. Geological Society of America Bulletin 82, 2933–2944.

Smith, D.L., Miller, E.L., Wyld, S.J., Wright, J.E., 1993. Progression and timing of Mesozoic crustal shortening in the northern Great Basin, western USA. In: Dunne, G., McDougall, K. (Eds.). Mesozoic Paleogeography of the Western United States-II. Pacific Section SEPM, pp. 389–406 Book 71.

Snoke, A.W., Miller, D.M., 1988. Metamorphic and tectonic history of the northeastern Great Basin. In: Ernst, W.G. (Ed.). Metamorphism and Crustal Evolution, Western Coterminous United States, Vol. 7. Prentice-Hall, Englewood Cliffs, NJ, pp. 606–648.

Speed, R.C., 1974. Evaporite–carbonate rocks of the Jurassic Lovelock Formation, West Humboldt Range, Nevada. Geological Society of America Bulletin 85, 105–118.

Speed, R.C., 1978. Paleogeographic and plate tectonic evolution of the Early Mesozoic marine province of the Western Great Basin. In: Howell, D.G., McDougall, K.A. (Eds.). Mesozoic Paleogeography of the Western United States. SEPM, pp. 253–270 Pacific Coast Paleogeography Symposium 2.

Spry, A., 1969. Metamorphic Textures. Pergamon Press, New York.

Stewart, J.H., Carlson, J.E., 1978. Geologic map of Nevada. Nevada Bureau of Mines and Geology, scale 1:500,000.

Thole, R.H., Prihar, D.W., 1998. Geologic map of the Eugene Mountains, northwestern Nevada. Nevada Bureau of Mines and Geology Map, 115.

White, S.H., Knipe, R.J., 1978. Microstructure and cleavage development in selected slates. Contributions to Mineralogy and Petrology 66, 165–174.

Wyld, S.J., 1996. Early Jurassic deformation in the Pine Forest Range, northwest Nevada, and implications for Cordilleran tectonics. Tectonics 15, 566–583.

Wyld, S.J., 1998. Structural development of the Luning–Fencemaker fold-and-thrust belt: new constraints from northern Nevada. Geological Society of America Abstracts with Programs 30, 62.

Wyld, S.J., 2000. Triassic evolution of the arc and back-arc of northwest Nevada, and evidence for extensional tectonism. In: Soreghan, M.J., Gehrels, G.E. (Eds.). Paleozoic and Triassic Paleogeography and Tectonic Evolution of Western Nevada and Northern California. Geological Society of America, Boulder, CO, pp. 1–23 Special Paper 347.

Wyld, S.J., Wright, J.E., 2000. Timing of deformation in the Mesozoic Luning–Fencemaker fold-thrust belt, Nevada. Geological Society of America Abstracts with Programs 32, no. 7, A169–A170.

Wyld, S.J., Copeland, P., Rogers, J.W., 1999. $^{40}Ar/^{39}Ar$ whole rock phyllite ages from the Mesozoic Luning–Fencemaker thrust belt of central Nevada. EOS, Transations of the American Geophysical Union 80 (46), F977.

Yardley, B.W.D., 1990. An Introduction to Metamorphic Petrology. Longman Scientific and Technical, Essex, England.